Ore Geology Reviews 89 (2017) 96–113

Contents lists available at ScienceDirect

Ore Geology Reviews

journal homepage: www.elsevier.com/locate/oregeo

Geological and geochemical constraints on the Cheshmeh-Frezi volcanogenic stratiform manganese deposit, southwest Sabzevar basin, Iran

Sajjad Maghfouri [a], Ebrahim Rastad [a,*], Fardin Mousivand [b], Flavien Choulet [c], Lin Ye [d]

[a] Department of Geology, Faculty of Basic Sciences, Tarbiat Modares University, Tehran, Iran
[b] School of Geosciences, Shahrood University of Technology, Shahrood, Iran
[c] Chrono-Environnement, Université de Franche-Comté/CNRS, 25030 Besançon cedex, France
[d] State Key Laboratory of Ore Deposit Geochemistry, Institute of Geochemistry, Chinese Academy of Sciences, Guiyang 550002, China

ARTICLE INFO

Article history:
Received 21 February 2017
Received in revised form 9 June 2017
Accepted 12 June 2017
Available online 13 June 2017

Keywords:
Manganese
Cheshmeh-Frezi
Volcano-sedimentary sequence
Late Cretaceous
Cuban-type
Sabzevar zone

ABSTRACT

The Cheshmeh-Frezi Mn deposit belongs to the southwest Sabzevar basin to the north of the Central Iranian microcontinent. This basin, which hosts abundant mineral deposits including Mn exhalative and Besshi-type Cu-Zn volcanogenic massive sulfide deposits, followed an evolution closely related to the subduction of the Neo-Tethys oceanic crust beneath the Central Iranian microcontinent. Two major sedimentary sequences are recorded within this basin: (I) the Lower Late Cretaceous volcano-sedimentary sequence (LLCVSS) and (II) the Upper Late Cretaceous sedimentary dominated sequence (ULCSS). The Cheshmeh-Frezi Mn deposit is hosted within red tuff with interbeds of green tuffaceous sandstone of the LLCVSS. Mineralization occurs as stratiform blanket-like and tabular orebodies. Psilomelane, pyrolusite and braunite are the main minerals of the ore, which display a variety of textures. Such as layered, laminated, disseminated, massive, replacement or open space fillings. The footwall and hanging-wall volcanic rocks are predominantly andesite and trachyandesite rocks. Footwall and hanging-wall volcanic rocks at Cheshmeh-Frezi are enriched in light rare earth elements (LREEs) compared to chondrite, have steep REE patterns, and generally show Ta and Nb depletions relative to chondrite which are characteristic of back-arc environments. The significant geochemical characteristics of ore such as high Mn content (12.41–33.14 wt%; average 19.41 wt%), low concentration of Fe (0.64–2.27 wt%; average 1.63 wt%), high Ba (49.7–9901 ppm, average 2728.67 ppm), LREE > HREE, and negative Ce and Eu anomalies reveal a primary distal hydrothermal-exhalative source for mineralization. Cheshmeh-Frezi deposit, in comparison with different types of volcanogenic manganese deposits shows broad similarities with the Cuban-type Mn deposits such as tectonic, host and associated rock types, geometry, textures, structures, mineralogy and lithogeochemistry.

1. Introduction

Manganese (Mn) deposits can be formed by various sedimentary, hydrothermal, hydrogenous, and supergene processes. Hydrothermal Mn deposits are generally smaller in size and economic importance relative to sedimentary ones (Roy, 1992; Frakes and Bolton, 1992). Hydrothermal Mn ores formed by the precipitation of low-temperature hydrothermal solutions at the origin of generally stratabound to irregular orebodies and veins (Roy, 1992; Nicholson, 1992; Kuleshov, 2011). They are found throughout the geological epochs, in different tectonic settings, from marine environments close to spreading centers, to intra plate seamounts, or subduction-related island arcs, (Roy, 1997). Conversely, stratiform sedimentary deposits, which may reach world-class importance with hundreds of million tons, display oxide–carbonate phases formed in the organic-rich sediments deposited onto the continental shelves during transgression–regr ession ecents in a greenhouse–icehouse climate, as exemplified by the Chiatura (Georgia) and Nikopol (Ukraine) giant deposits (Roy, 2006).

In Iran, different types of Mn and Fe-Mn ore deposits are recognized in different geological settings, and they range from Precambrian/Early Cambrian to Late Miocene/ Pliocene (Fig. 1).

* Corresponding author.
E-mail addresses: Maghfouri64@yahoo.com (S. Maghfouri), rastad@modares.ac.ir (E. Rastad), fmousivand@yahoo.com (F. Mousivand), flavien.choulet@univ-fcomte.fr (F. Choulet), yelin@vip.gyig.ac.cn (L. Ye).

http://dx.doi.org/10.1016/j.oregeorev.2017.06.015
0169-1368/

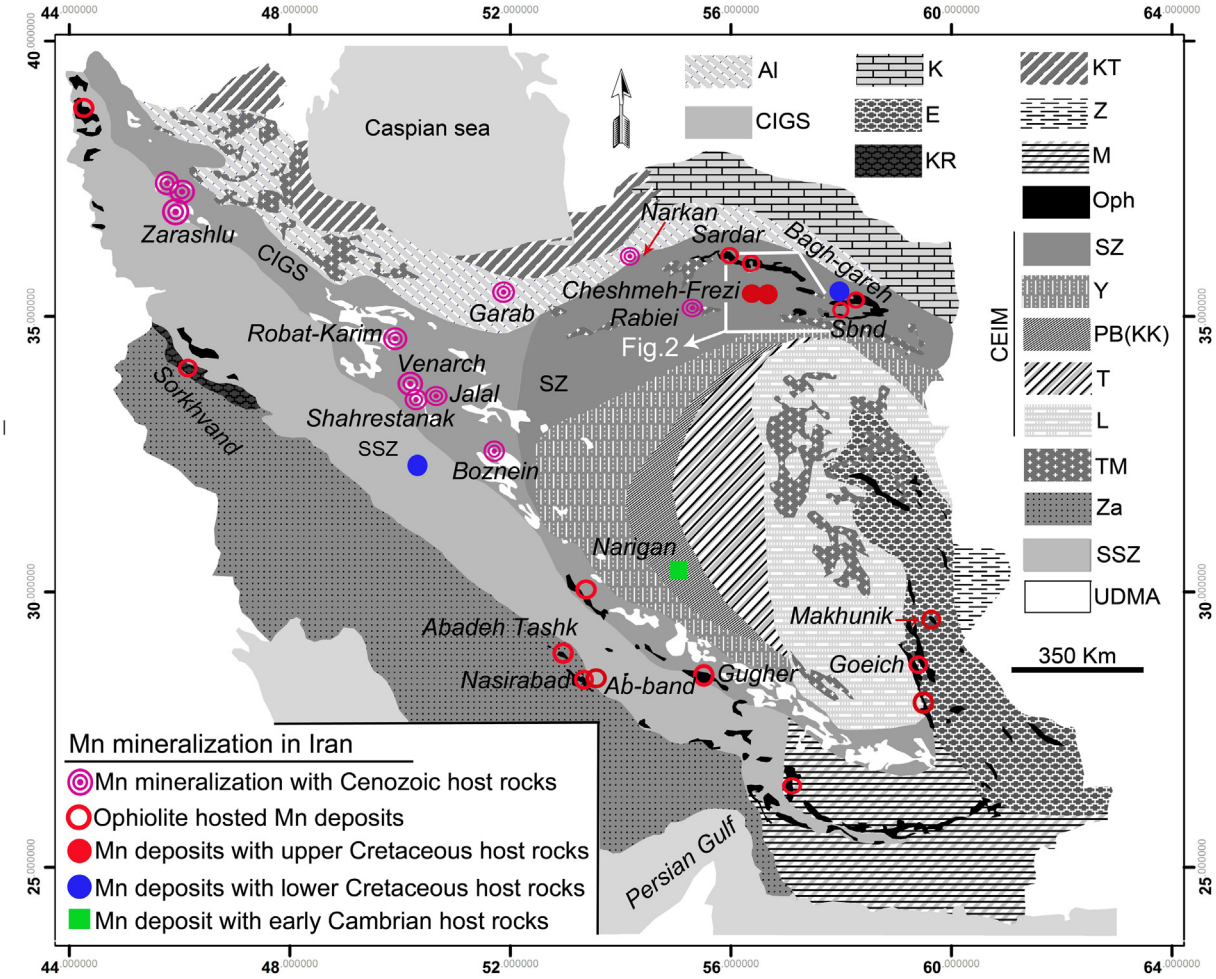

Fig. 1. Distribution map of manganese deposits according to the age of host rocks in the main tectonic elements of Iran (Outlined rectangle is the area shown in Fig. 2); CIGS, Central Iranian geological and structural gradual zone; E, East Iran ranges; K, Kopeh-Dagh; KR, Kermanshah Radiolarites subzone; KT, Khazar-Talesh- Ziveh structural zone; L, Lut block; M, Makran zone; O, ophiolite belts; PB, Posht-e-Badam block; SSZ, Sanandaj-Sirjan zone; T, Tabas block; TM, tertiary magmatic rocks; UD, Urumieh-Dokhtar magmatic arc; Y, Yazd block; Z, Zabol area; Za, Zagros ranges (tectonic and structural map of Iran modified after Aghanabati, 1998, 2004 and Alavi, 1996).

- In Central Iran, the Infracambrian Narigan Mn ore deposit in Posht-e-Badam block has a volcano-exhalative origin (Bonyadi and Moore, 2005 Rajabi et al., 2014).
- In different areas of Iran, Lower Cretaceous sedimentary sequence hosts Mn and Mn-Fe mineralization, with the examples of the Bagh-gareh, Chah basheh and Shamsabad deposits (Ahmadi, 2006).
- Cretaceous ophiolitic Mn deposits are found in the Khoy, Kermanshah (Sorkhvand deposit), Neyriz (Nasirabad deposit), Nain (Benvid deposit), Sistan (Kamar Talar deposit) and Sabzevar (Sardar deposit) ophiolitic belts (Arvin and Robinson, 1994; Emamalipour, 2010; Zarasvandi et al., 2013, 2016b; Hosseini and Mousivand, 2016)
- The late Cretaceous volcano-sedimentary sequence in the southwest of the Sabzevar basin (Fig. 2) hosts several Mn deposits (e.g. Cheshmeh-Frezi; Benesbourd; Homaei; Nudeh; Zeiheri; Goft; Cheshmeh-saefid, Danaei and Zakeri) (Masoudi, 2008; Maghfouri, 2012; Nasrollahi et al., 2012; Taghizadeh et al., 2012; Maghfouri et al., 2015)
- In the northern part of Iran, many major Mn and Mn-Fe deposits such as Venarch, Shahrestanak, Robat-Karim, Qaleh Mohammad Khan, Jokandi and Garab deposits occurred within the Cenozoic volcano-sedimentary sequence rocks, especially within the andesitic-dacitic lavas (Amiri, 1995; Doulatkhah et al., 2005; Malekghasem and Simmonds, 2006; Heshmatbehzadi and Shahabpour, 2010; Maghfouri et al., 2015; Mahdavi et al., 2015; Nabatian et al., 2015; Zarasvandi et al., 2016a; Zarasvandi et al., 2016b; Rajabzadeh et al., 2017).

The Cheshmeh-Frezi Mn deposit is located 95 km to the southwest of Sabzevar city, northeastern Iran (Fig. 2). It has been described as an exhalative deposit (Maghfouri, 2012), exposing a 6 to 20 m-thick and 2300 m-long mineralized orebody. It has been mined discontinuously from ancient times until to the present day. The Cheshmeh-Frezi deposit exposes both lenses and stratiform orebodies, which occurs within a Lower Late Cretaceous bimodal volcano–sedimentary sequence (Figs. 3 and 4) (Maghfouri, 2012; Maghfouri et al., 2015). The southwest Sabzevar basin also hosts the Nudeh Cu-Zn Besshi-type VMS deposit (Maghfouri et al., 2016), 4 km to south of the Cheshmeh-Frezi (Fig. 3). The spatial relationship between Cu-Zn and Mn mineralization has not been studied in detail, even though both types of mineralization are hosted by the same volcano-sedimentary formation.

Presently, no detailed investigation on the origin of the Mn mineralization from the Cheshmeh-Frezi deposit is available. Recently, Maghfouri et al. (2016) proposed a model to explain the genesis of the Nudeh Cu-Zn Besshi-type VMS. On the basis of field observations and new major, trace, and rare-earth element (REE) geochemical data, this paper aims at discussing the genesis of Mn ore mineralization and the typology of the Cheshmeh-Frezi deposit.

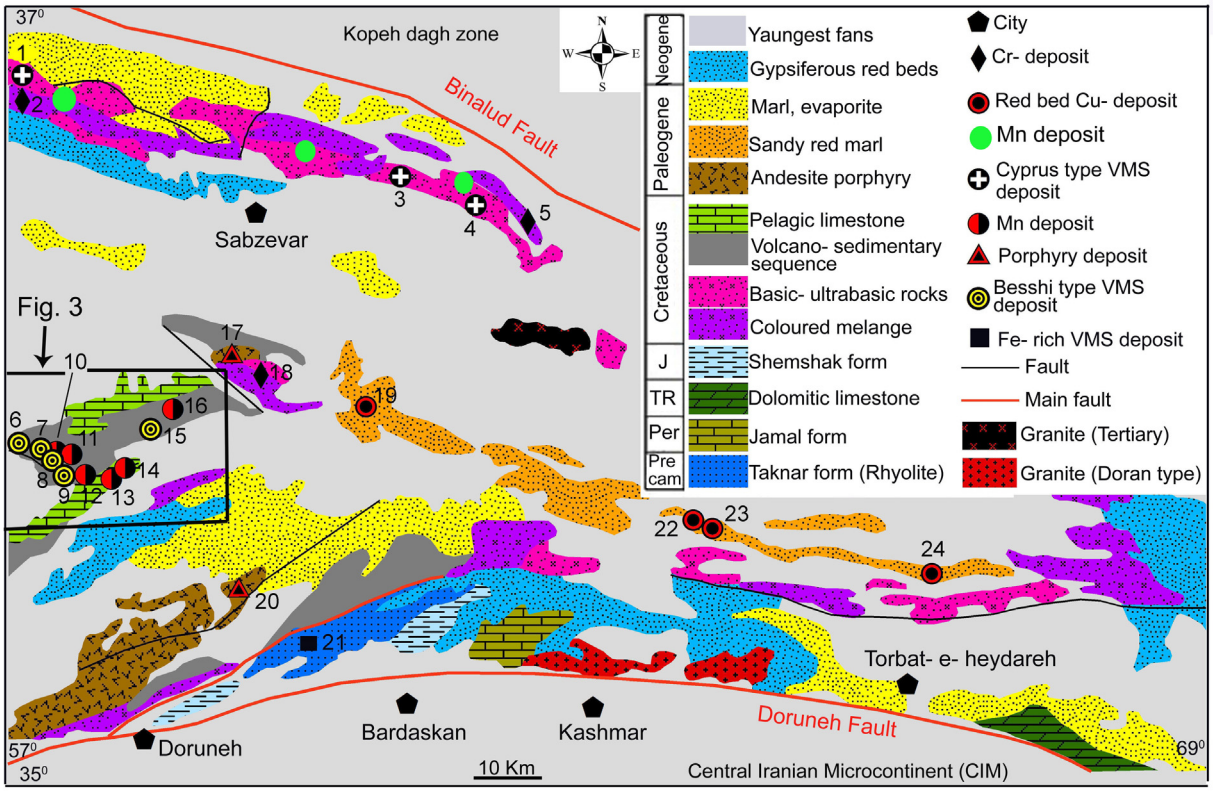

Fig. 2. Distribution map of deposits in the eastern segment of the Sabzevar zone. Most of manganese deposits occur in the Cretaceous rocks (modified after Emami et al., 1993).1 and 2. Olang sar; 3. Sozandeh; 4 and 5. Goudesag; 6. Garab; 7. Kalateh Lala; 8. Cheshmeh-Frezi; 9. Nudeh: 10. Cheshmeh-Frezi; 11. Benesbord; 12. Nudeh; 13. Cheshmeh safed; 14. Zakeri; 15. Chun; 16. Goft; 17. Halakabad; 18. Tondak; 19. Dahmian; 20. Dahan galaeh; 21. Taknar; 22. Sfeiz; 23. Kadkan; 24. Rodkhaneh (Outlined rectangle is the area shown in Fig. 3).

2. Stratigraphy of the southwest Sabzevar basin

The Cheshmeh-Frezi Mn deposit is located in the southwest Sabzevar basin, within the northeastern segment of the Sabzevar zone (SZ), a tectonic domain wedged between the Central Iranian Microcontinent (CIM) to the south and the Kopeh Dagh sedimentary basin to the north (Fig. 2). The southwest Sabzevar Basin is characterized two successive sedimentary sequences: 1) the Lower Late Cretaceous volcano-sedimentary sequence (LLCVSS), including fine-grained siliciclastic sediments and bimodal volcanics and pyroclastic rocks, and 2) the Upper Late Cretaceous Sedimentary dominated Sequence (ULCSS), formed by pelagic limestone, marly tuff, silty limestone and marl (Fig. 4) (Maghfouri, 2012; Maghfouri et al., 2016). To the southwest of the basin, in the Sabzevar zone, the volcano-sedimentary sequences are deformed due to post-Cretaceous compression and expose an anticline extending 8 to 14 km in width and about 100 km in length (Fig. 3). The overall strike of the structure is broadly SW-NE, parallel to the general regional trend of the Sabzevar zone (Maghfouri, 2012).

2.1. The Lower Late Cretaceous volcano-sedimentary sequence (LLCVSS)

Representative stratigraphic columns of the southwestern part of the Sabzevar basin are shown in Fig. 4A. In this basin, the LLCVSS (with an overall maximum thickness of 1320 m) unconformably overlies the Lower Cretaceous formations (Fig. 4A) (Maghfouri, 2012). The LLCVSS is characterized by: (a) abrupt changes of facies and thickness, (b) wedge-shaped basin fill geometry, (c) bimodal volcanism, and (d) a typical rift-related sedimentary sequence. Maghfouri (2012) divided this sequence into three different units from bottom to top (Fig. 4A):

(1) The basal sedimentary unit (Unit 1), mainly exposed to the S and SE of the Cheshmeh-Frezi and Nudeh areas, consists of shallow marine gray lithic tuff, rhyolite flow, andesitic tuff, andesite (hosting Cu mineralization at Garab and Cheshmeh-Frezi), red tuff (hosting Mn mineralization at Nudeh, Benesbourd, Cheshmeh-Frezi and Goft), trachyandesite, pillow lava and dacite porphyry (Maghfouri, 2012; Maghfouri et al., 2016). This unit displays abrupt changes in thickness, reaching 630 m in the Nudeh syncline but tapers rapidly eastward, as it approaches the edge of the basin. Unit 1 is characterized by bimodal mafic volcanics, including rhyolite, dacite, andesite and basaltic pyroclastic rocks (Maghfouri, 2012; Maghfouri et al., 2016).
(2) Unit 2 is composed of a 390 m-thick sequence of agglomerate, lapilli tuff, gabbro sill, alkali olivine basalt flow with minor tuffaceous silty sandstone (Fig. 4A). The basalt flow laterally changes to tuffaceous silty sandstone, which hosts the Besshi-type VMS Cu-Zn orebodies at Nudeh, Chun and Lala (Maghfouri et al., 2016). According to these authors, the Nudeh VMS Cu- Zn deposit occurs at the site of the maximum thickness for the sequence of alkali olivine basalt and tuffaceous silty sandstone, at site of *syn*-sedimentary faulting. This ore-bearing interval is covered by banded shale and tuffaceous shale, forming a key layer for stratigraphic correlation in the LLCVSS (Maghfouri, 2012).
(3) The upper member (Unit 3) of the LLCVSS includes a series of green to gray pyroclastic rocks (up to 700 m thick) and minor shales and sandstones (Fig. 4A). Within units 2 and

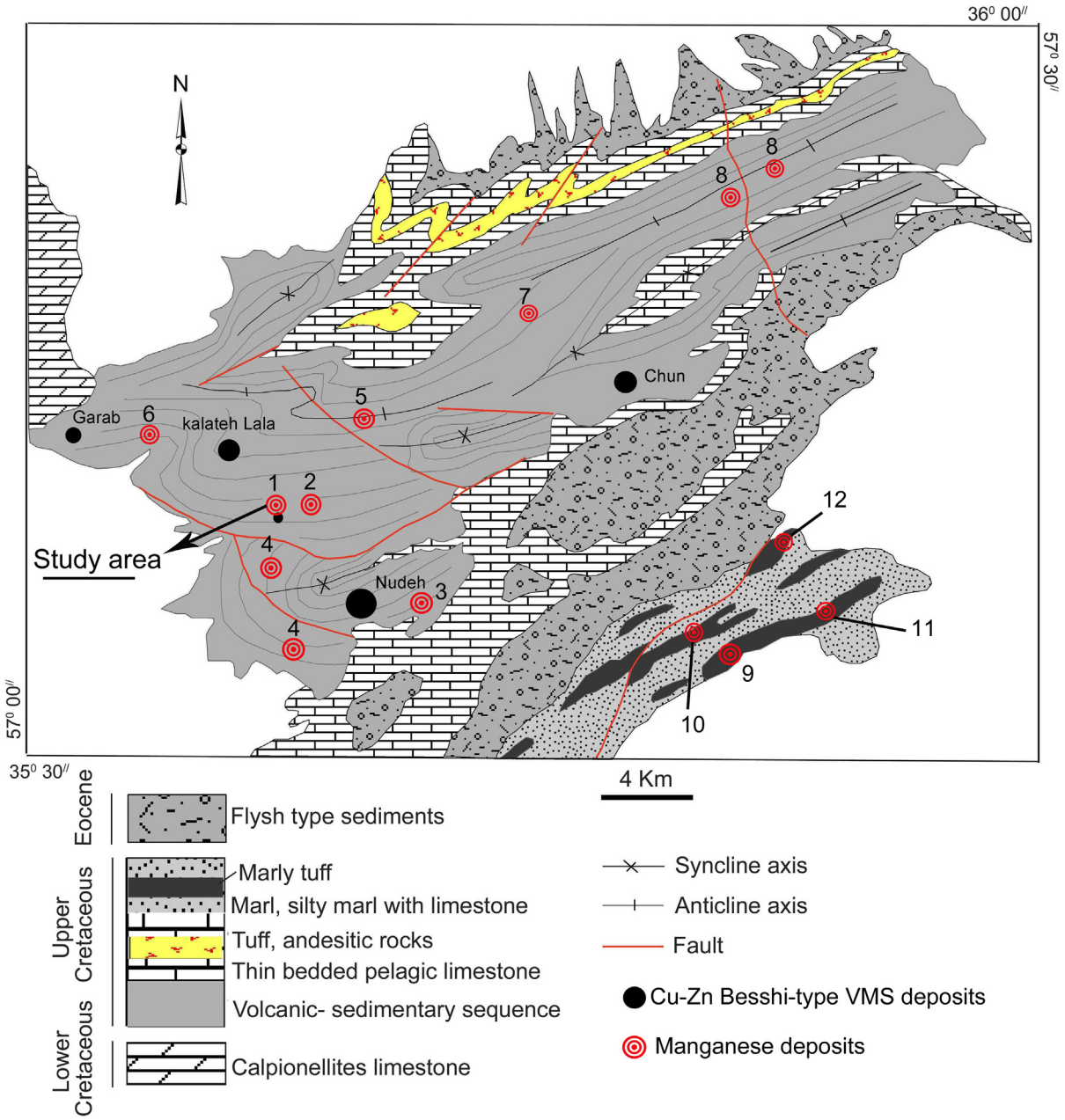

Fig. 3. Simplified geological map of the Southwest Sabzevar basin, showing the location of manganese and Besshi-type VMS deposits within this basin. 1: Cheshmeh-Frezi, 2: Benesbourd, 3: Nudeh, 4: Khavarzamin, 5: Homaei, 6: Lala, 7: Zeiheri, 8: Goft, 9: Cheshmeh-saefid, 10; Zakeri1, 11: Zakeri2; 12: Danaei.

3, gabbro sills, contemporaneous with sediments and pyroclastic, are exposed in the southern and northeastern parts of the basin, especially in the Nudeh and Kalmorgh areas.

2.2. The Upper Late Cretaceous sedimentary sequence (ULCSS)

Unit 3 of the LLCVSS grades upward into the ULCSS (Unit 4) composed, from bottom to top, of Globotruncana-bearing pelagic limestone, marly tuff, sandy limestone and silty marl with interbedded limestone (Fig. 4A) (Maghfouri, 2012; Maghfouri et al., 2016). Economic Mn deposits, like Cheshmeh Saefid, Zakeri and Danael occur within the marly tuff in the southeastern part of the basin (Figs. 2–4A). A major change in the sedimentary regime is required to explain the transition from the siliciclastic (with associated bimodal volcanism) LLCVSS to the calcareous to marly ULCSS. This change reflects the Late Cretaceous evolution of the basin marked by the progressive infilling of the rift (Betts et al., 1998; Large et al., 2002). The ULCSS strata can be followed over large distances in the southwestern part of the Sabzevar basin, showing less lateral changes of the facies compare to those of the LLCVSS (Maghfouri, 2012; Maghfouri et al., 2016).

3. Local stratigraphy of the Cheshmeh-Frezi deposit

Unit 1 of the LLCVSS has a maximum thickness of 310 m, and is exposed mainly in the Cheshmeh-Frezi district (Fig. 4B). The stratigraphic succession is composed of sedimentary-derived clastic and pyroclastic rocks in the lower part, and basic to intermediate lava

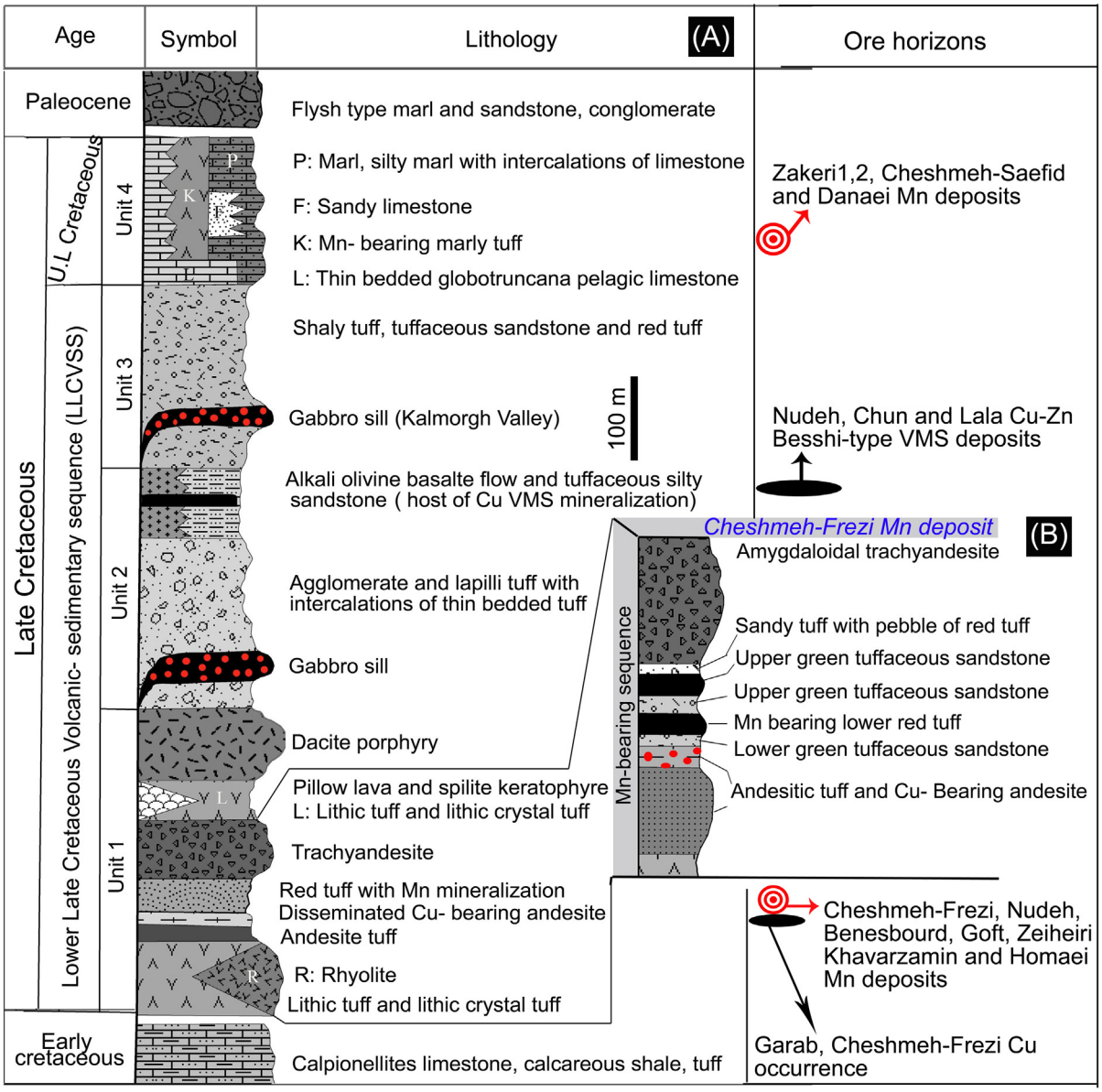

Fig. 4. A: Generalized schematic columnar section of the Cretaceous sequence of the southwest Sabzevar basin, with the main ore-bearing strata. B: stratigraphic sequence of the Unit1 (ore-bearing Unit), red tuff of this unit is host rock of manganese in the Cheshmeh-Frezi deposit.

flows in the upper part (Fig. 4B) (Maghfouri, 2012). The thickness of the flows and the ratio between lava and pyroclastic rocks increase upwards. The lowermost lithic tuff and lithic crystal tuff, has a minimum thickness of 12 m (Fig. 5A). It is overlain by a sequence of andesitic tuff and andesite flow (hosting disseminated Cu occurrences), characterized by a distinctive green to rarely gray color and thick to medium bedding (Fig 5A). The maximum thickness of these rocks is about 100 m. Overlying the andesite flow is an up to tens of meters-thick red tuff and green tuffaceous sandstone. The lower and upper red tuff layers alternately changes into green tuffaceous sandstone sediments, which host the Mn orebody, of the Cheshmeh-Frezi deposit (Fig. 4B). The occurrence of layering and volcanic clasts in the pyroclastic rocks provides good evidence of their formation by explosive eruptions in a shallow marine sedimentary basin (Asiabanha et al., 2012). The Mn-bearing upper red tuff is covered by sandy tuff with pebbles of red tuff (Fig. 5B). This sequence is overlain by amygdaloidal trachyandesite flows, with a maximum thickness of about 110 m (Figs. 4B and 5A).

4. Methodology

The present study investigates the mineralogy and paragenetic sequence of the Cheshmeh-Frezi deposit on the basis of the optical microscopic observation of 26 polished thin and thick sections. Supplementary investigations were carried out using a FEI/Philips XL30 scanning electron microscope at Tarbiat Modares University, Iran. In order to correctly characterize their chemical compositions, 20 samples were selected for major, trace, and rare-earth-elements (REE) analysis. Rock chips (~400 g) from each sample were carefully sampled, washed with distilled water at room temperature, and then dried. They were further crushed and powdered in tungsten carbide swing mill. Bulk-rock chemical analysis of major, trace, and REE elements were determined for all samples by Inductively Coupled Plasma-Emission Spectrometry (ICP-ES) and Mass Spectrometry (ICP-MS) at Institute of Geochemistry, Chinese Academy of Sciences, Guizhou, China.

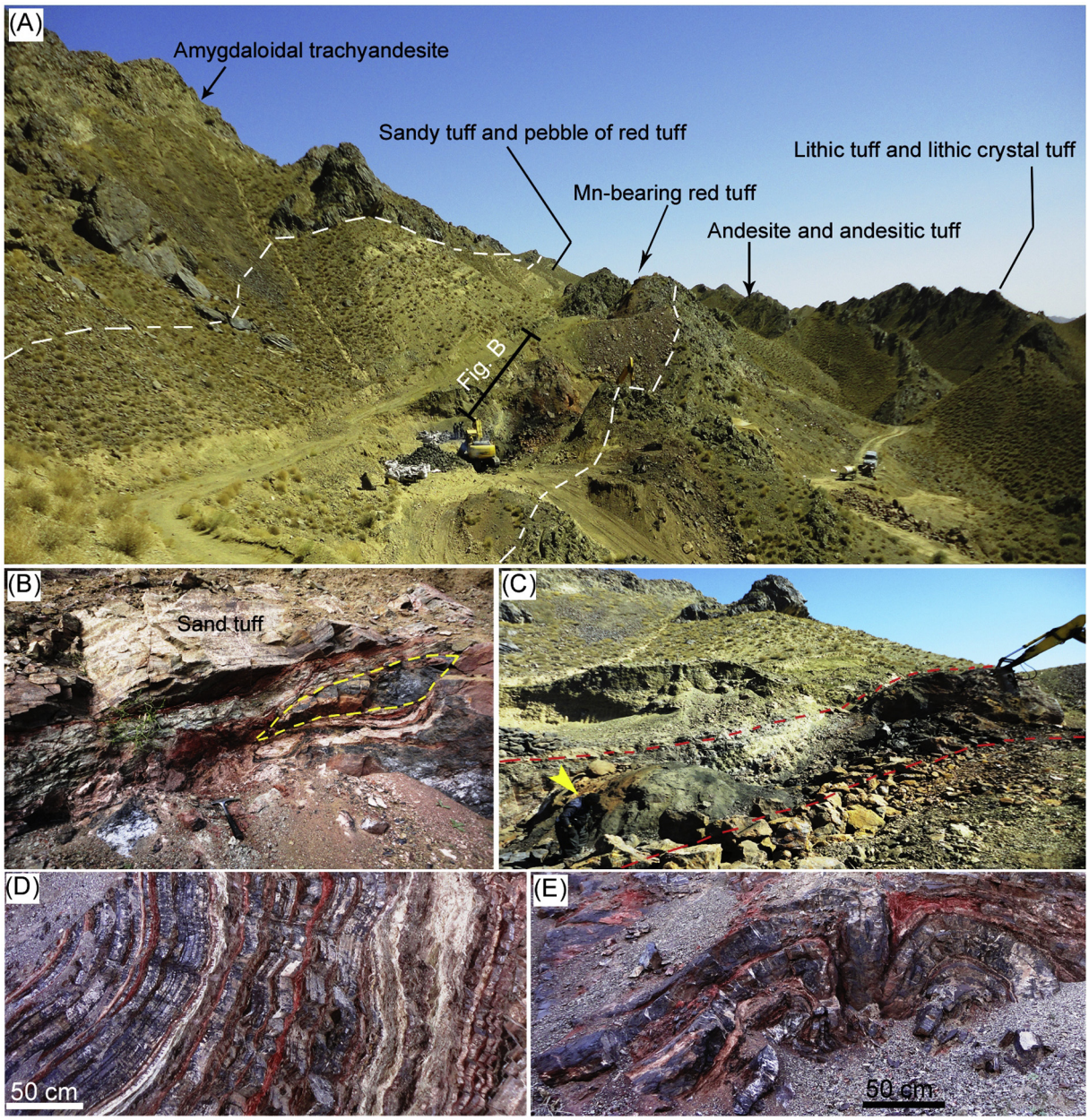

Fig. 5. Photographs of the Cheshmeh-Frezi Mn deposit. A: The location of ore-bearing red tuff that is embedded with andesite flow and sandy tuff. B: Outcrop of red tuff overlain by sandy tuff. C: View of the manganese layer between underlying andesite and overlying sandy tuff. D) Outcrop of manganese ore layers with interbedded of red tuff. E) Ore layers (black) and red tuff folded to form of anticline.

5. Manganese mineralization

The Cheshmeh-Frezi Mn mineralization is recognized by their black color in the field (Fig. 5). It consists of two different mineralized layers, namely Mn-bearing lower red tuff (LRT) and Mn-bearing upper red tuff (URT) (Figs. 4B and 5). The thickness of these Mn-bearing layers in the Cheshmeh-Frezi mine range between 6 and 20 m; they are separated by barren interbeds of sandy tuff, tuffaceous sandstone and tuff (Figs. 4B and 5B). The total thicknesses of the ore-bearing rock layers are positively correlated with the thickness of each ore body. These orebodies occur as bedded and lenticular shapes (Fig. 5C), and their texture is controlled by the host strata. The Mn grades vary between 16% and 42%. Compared to the lower orebodies, the upper ones are thicker and show higher Mn grade. Best grades are generally in the basal part of the upper orebodies, although secondary enrichment also occurs along late faults. The trend of the mineralization is SW–NE, dipping 20°-30° to the northwest, consistent with the bedding of the host rock. The mineralized layers (laminate and bands) are locally folded and cut by the fault and micro-fractures (Figs. 5D and 5E), indicating a role of tectonics during post-sedimentartion episodes. The most abundant minerals within the LRT and URT are psilomelane, pyrolusite and braunite (Figs. 6 and 7). The gangue minerals are mainly quartz, feldspar and chlorite, which coexist with lithic clasts in the tuff. Textures and structures of ores involve layered (Fig. 5C and D), laminated (Figs. 6 and 7), disseminated, massive, replacement and open space fillings. The massive ores, mainly in the upper orebodies, are of higher grades and composed of psilomelane and pyrolusite. Two types of banded ores have been recognized. While a first laminated type is formed by 1–10 cm thick laminaes

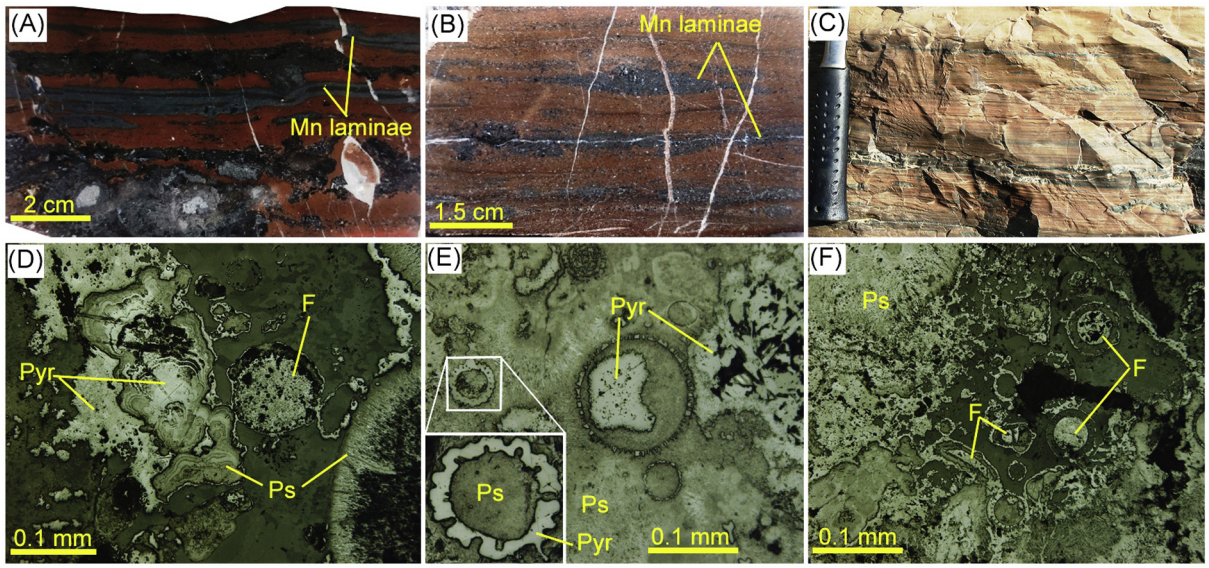

Fig. 6. Hand specimen (A, B and C) and reflected light microscopic (D, E and F) photographs of the manganese ore minerals in the Cheshmeh-Frezi deposit. A and B: banded (laminated) texture, where the laminaes are 0.1–1 cm and mainly composed of red tuff and manganese ore minerals (black laminae). C: Photograph of typical manganese laminae (black) and red tuff. D: Reflected light image of manganese minerals consisting of psilomelane (Ps) and pyrolusite (Pyr). Replacement of fossil with psilomelane is shown. E and F: Photomicrograph of Globotruncana foraminifera fossil that has been largely replaced by pyrolusite (Pyr) and minor psilomelane (Ps).

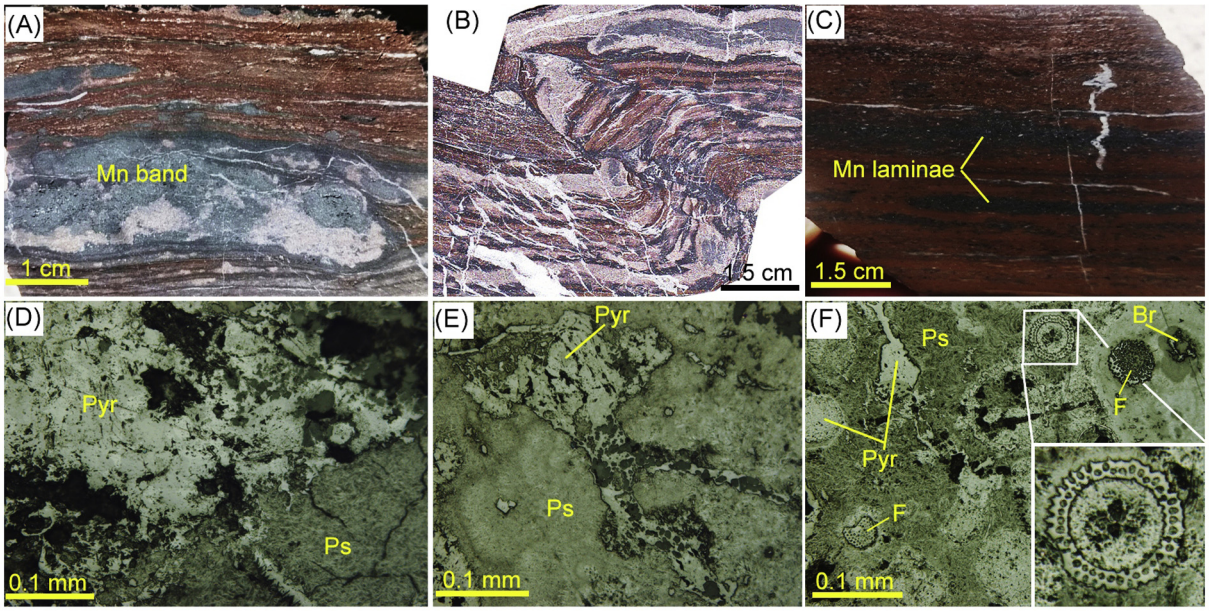

Fig. 7. Hand specimen (A, B and C) and reflected light microscopic (D, E and F) photographs of the manganese ore minerals in the Cheshmeh-Frezi deposit. A: Typical massive thick-banded manganese ore. B: laminated texture, where the laminaes are folded and mainly composed of red tuff and manganese ore minerals (black laminae). C: Photograph of typical manganese laminae (black) and red tuff. D and E: Reflected light image of manganese minerals consisting of psilomelane (Ps) and pyrolusite (Pyr). Replacement of fossil with psilomelane is shown. F: Photomicrograph of Globotruncana foraminifers' fossil that has been largely replaced by pyrolusite (Pyr) and minor psilomelane (Ps) and braunite (Br).

(Figs. 5D, 6 and 7), a second type is characterized by thicker (up to 10 cm) Mn layers (Fig. 5E). The disseminated Mn minerals occur commonly as a low-grade mineralization within the barren red tuff and the lower part of the host rock. Open-space filling textures formed, as ores experienced brittle deformation, followed by secondary precipitation of manganese minerals. Replacement of Cretaceous pelagic fossil by psilomelane, pyrolusite and braunite is also frequently observed in the Cheshmeh-Frezi deposit (Figs. 6 and 7).

6. Whole-rock geochemistry

In the case of ore deposit geochemistry, major element abundances are of limited use, as most of them (especially alkalis) are susceptible to modification during hydrothermal alteration (Peter and Scott, 1999; Peter et al., 2014). In the example of Cheshmeh-Frezi, we may observe iron enrichment associated with mineralization (Fig. 8A). Data from volcanic rocks collected in the foot- and hanging-wall plot distinctly within the tholeiitic field of Fig. 8A.

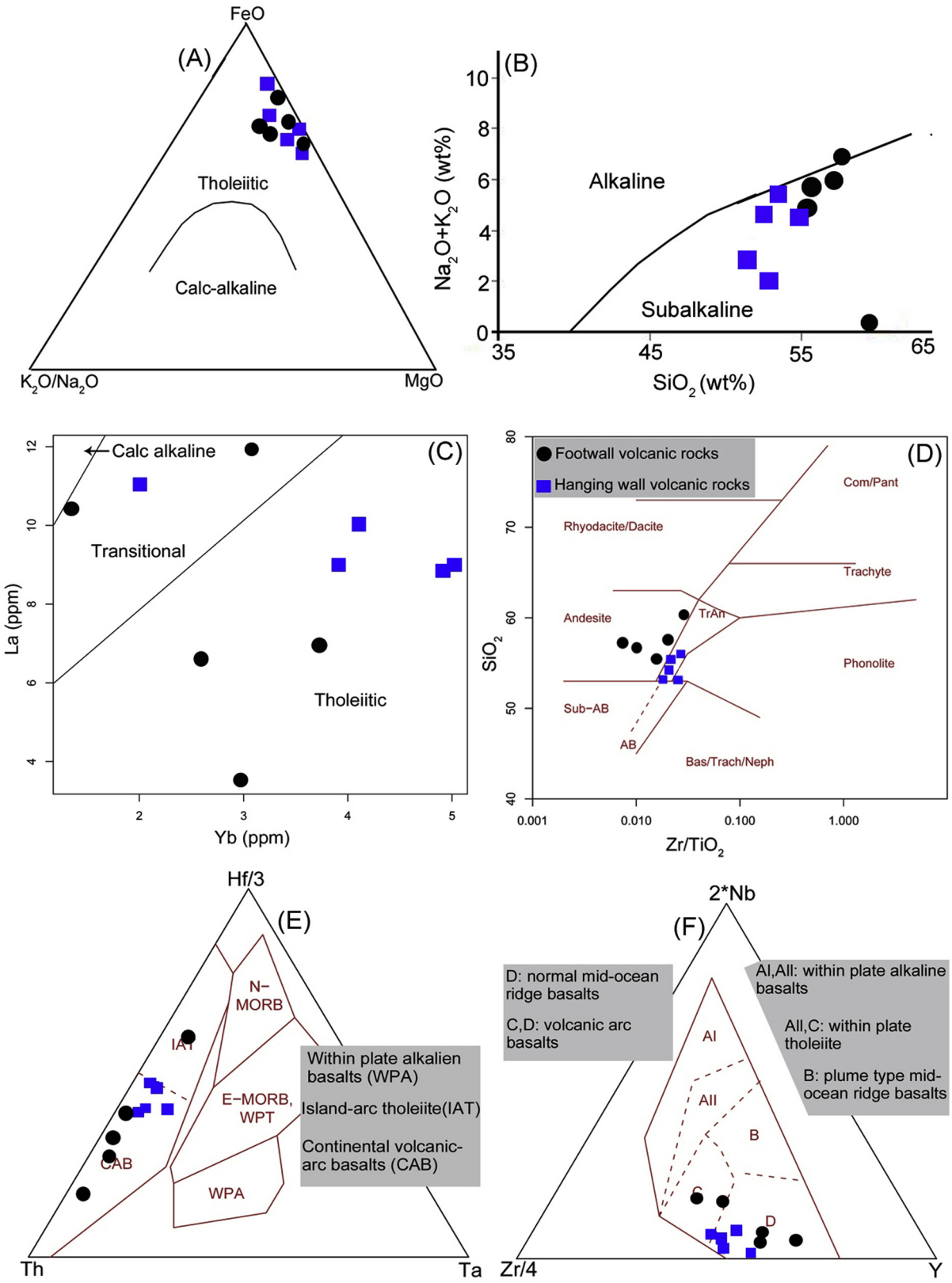

Fig. 8. A: AFM plot showing calc-alkaline and tholeiitic fields (Irvine and Baragar, 1971) and Fe-enrichment for Cheshmeh-Frezi volcanic rock samples. B: Plot of SiO2 versus NaO + K2O for igneous rocks showing alkaline and subalkaline fields of Irvine and Barager (1971). C: La vs. Yb diagram showing the generally less calc-alkaline character for the hangingwall volcanic rocks compared to those from the footwall; Subdivisions from Barrett and MacLean (1999). D: Selected discrimination diagrams for volcanic rocks of the Cheshmeh-Frezi deposit. A classification using the Zr/TiO2 vs. SiO2 diagram of Winchester and Floyd (1977) distinguishes between volcanic rocks. E: Hf/3-Th-Ta ternary diagram of Wood (1980), is showing dominantly island arc tholetitic (IAT) basalts and continental volcanic arc basalt (CAB). F: Zr/4–2Nb–Y ternary diagram of Meschede (1986) is showing dominantly volcanic arc basalt (VAB).

However, this may be interpreted as a result of alteration of the primary composition, as hanging wall samples were collected far from the deposit, compare to those of the footwall and, hence, are commonly less altered. On the$Na_2O + K_2O$ vs. SiO_2 plot (Fig. 8B) of Irvine and Baragar (1971), data for the volcanic rocks (footwall and hanging wall) fall predominantly within the subalkaline field, with some on the dividing line. but a large number of samples display a severe depletion in Na and K due to hydrothermal alteration.

Conversely, geochemistry of immobile trace and rare earth elements is a classical tool to track primary process and may be used to determine the tectonic setting of volcanic rocks hosting the ore deposit. Except for two outliers, the footwall volcanic rocks, display lower La/Yb value compare to the rocks of the hanging-wall. All of the collected samples plot in the fields of tholeiite and transitional (Fig. 8C). The positive correlations between Zr, Ti, and P and MgO, Cr, and Ni, together with the constant ratios between high field strength elements (HFSE), such as Zr, Hf, Nb and Ta indicate that these elements have not been significantly mobilized during hydrothermal alteration (Peter et al., 2014). On the log (Zr/TiO_2) vs. SiO_2 plot of Winchester and Floyd (1977), all the data plot within the andesite and trachyandesite fields (Fig. 8D). Thorium is immobile under submarine hydrothermal alteration conditions, equivalent to the setting of the Cheshmeh-Frezi volcanic host rocks, and Th and Ta behave coherently in non subduction-related oceanic basalts, decoupling only in the subduction environment (Wood, 1980). In the Hf-Th-Ta ternary plot of Wood (1980), all the data from the footwall and hanging wall plot in the field of continental volcanic arc basalt (CAB), except for one sample that plot in the field of island-arc tholeiite (IAT) (Fig. 8E). On the Zr/4-Y-2∗Nb of Wood (1980), most of the Cheshmeh-Frezi volcanic rocks plot in the volcanic arc basalt field (Fig. 8F).

Fig. 9A-B shows MORB-normalized geochemical patterns (spider diagrams) arranged in order of increasing element compatibility, with the most incompatible elements plotted on the left. The shape of patterns on such plots is little-affected by differences in partial melting and fractional crystallization (Pearce, 2010, 2011); and variations may rather be explained in terms of heterogeneities in the mantle sources. The main incompatible element-depleted reservoir of convecting upper mantle is thought to yield flat patterns of normal mid-ocean ridge basalt (N-MORB), whereas the humped patterns are believed to be derived from incompatible element-enriched with "mantle plumes" (e.g., Tarney et al., 1980). Similarities in the patterns for the Cheshmeh-Frezi footwall and hanging wall volcanic rocks (Figs. 9A-B) suggest that they are derived from a common magma source.

Fig. 9C and D display chondrite-normalized REE abundance patterns for Cheshmeh-Frezi volcanic rocks of known tectonic setting for reference. All the spectra show that samples are enriched (around 10 times) in incompatible elements. The patterns for the footwall volcanics show significant variation from moderate to steep LREE enrichment. Most of the footwall and hanging wall volcanic rocks lack significant Eu anomalies, implying that little or no plagioclase fractionation occurred during magmatic processes. The Cheshmeh-Frezi volcanic rocks shows range from depleted N-MORB, through non-LREE depleted, to E-MORB. Such volcanic rocks have been found close to continents and have been related to the initial stages of back-arc spreading or back-arc rifting (Peter and Scott, 1999; Peter et al., 2014).

7. Discussion

7.1. Origin of the Cheshmeh-Frezi manganese deposit

Today's geochemical criteria to distinguish ferromanganese deposits of various origins are well established. Major element ratios, trace element concentrations and also enrichment effects

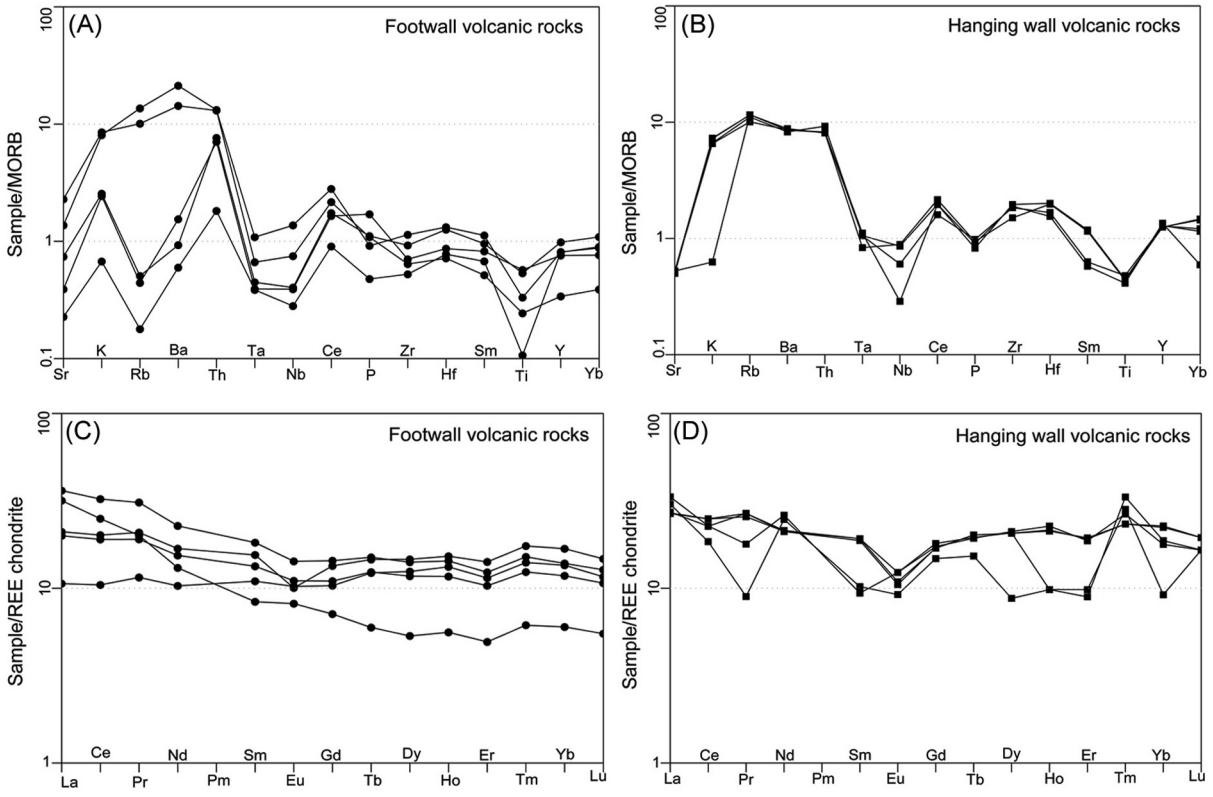

Fig. 9. A and B: Spider diagram of Cheshmeh-Frezi footwall and hangingwall volcanic rocks normalized to MORB (Pearce, 1983). C and D: Chondrite normalized (Nakamura, 1974) rare earth element plot for Cheshmeh-Frezi footwall and hangingwall volcanic rocks.

Table 1
Major oxides (wt.%) and trace elements (ppm) of Mn-ore, footwall and hanging wall volcanic rocks in the study area.

Sample	Rocks	SiO_2	Al_2O_3	Fe_2O_3	MgO	CaO	Na_2O	K_2O	MnO	P_2O_5	TiO_2	L.O.I.	Zr	Zn	Yb
1	Footwall volcanic rocks	60.22	13.37	6.92	1.8	4.92	0.24	0.1	11.7	0.05	0.16	0	47.18	122.9	2.98
2	Footwall volcanic rocks	57.26	14.25	7.99	2.82	2.9	5.03	0.36	2.41	0.2	0.85	5.4	63.35	53.3	2.59
3	Footwall volcanic rocks	56.65	15.79	9.69	2.36	6.08	4.88	0.38	0.26	0.13	0.8	0.6	83.23	23.06	3.7
4	Footwall volcanic rocks	55.56	17.86	8.7	2.28	6.03	3.58	1.27	0.12	0.13	0.36	3.3	57.63	65.59	1.32
5	Footwall volcanic rocks	57.69	12.31	10.9	4.34	3.1	5.93	1.2	0.04	0.11	0.49	4.2	102.4	55.47	3.05
6	Hanging wall volcanic rocks	55.24	11.08	13.97	2.9	0.96	3.11	1.09	0.12	0.11	0.65	10.24	135.5	41.17	4.9
7	Hanging wall volcanic rocks	54.24	12.08	11.97	4.9	0.96	5.11	0.09	0.12	0.11	0.65	9.24	135.5	41.17	5
8	Hanging wall volcanic rocks	53	14.07	13.97	5.15	0.8	3.27	1.08	0.13	0.10	0.66	8.24	176.5	0.17	3.91
9	Hanging wall volcanic rocks	54.1	15.17	14.99	4.13	4.00	1.07	0.98	0.23	0.11	0.61	7.24	170.5	6.17	2.01
10	Hanging wall volcanic rocks	52.1	13.1	12.9	5.29	6	2.03	0.99	0.22	0.12	0.71	8.24	165.4	11.27	4.11
11	Ore layers	56.96	1.46	3.25	2.53	6.64	0.53	1.25	20.7	0.18	0.01	5.39	15.27	82.83	1.15
12	Massive ore	43.95	0.8	2.19	0.93	4.33	0.29	0.02	42.8	0.15	0.11	4.16	36.5	47.1	2.2
13	Ore layers	55.71	1.19	0.92	0.59	9.89	0.29	0.01	20.29	0.05	0.06	10.5	36.01	47	1.4
14	Ore layers	58.4	0.56	1.99	0.96	5.02	0.24	0.75	24.41	0.09	0.04	6.7	33.8	23.8	2.4
15	Massive ore	40.01	2.36	3.01	1.05	6.89	0.22	1.03	39.98	0.08	0.6	4.02	16.5	13.3	4.2
16	Ore layers	54.15	3.02	2.8	2.08	7.56	0.62	1	19.6	0.17	0.3	8.21	47	50.04	1.3
17	Ore layers	62.12	6.9	1.91	0.88	5.39	0.91	0.65	18.01	0.1	0.02	6.65	18.2	43.02	0.2
18	Massive ore	48.29	2.67	3.01	1.61	4.09	0.15	0.09	29.31	0.06	0.2	9.62	2.3	111	2.2
19	Ore layers	61.96	1.74	2.53	1.01	6.23	0.82	0.87	19.69	0.12	0.03	4.37	36.2	37.5	0.3
20	Ore layers	68.08	1.08	1.9	1.5	4.88	0.37	0.02	16.03	0.12	0.19	5.32	72.8	56.03	1.4

Sample	Rocks	Y	W	V	U	Tm	Th	Tb	Ta	Sr	Sm	Sc	Sb	Rb	Pr
1	Footwall volcanic rocks	24.36	0.3	129.2	0.21	0.42	0.36	0.57	0.06	27.22	2.22	33.26	0.32	0.35	1.29
2	Footwall volcanic rocks	22.73	0.52	134.6	0.52	0.37	1.41	0.58	0.07	46.86	2.71	24.08	0.43	0.8	2.13
3	Footwall volcanic rocks	29.49	0.46	70.47	0.53	0.52	1.52	0.68	0.08	88.73	3.15	19.09	0.72	1.01	2.33
4	Footwall volcanic rocks	10.18	1.2	159.6	0.82	0.18	2.61	0.28	0.11	274.6	1.69	15.86	0.2	20.19	2.24
5	Footwall volcanic rocks	24.24	1	13.98	0.71	0.45	2.64	0.7	0.19	164.5	3.7	11.08	0.16	27.27	3.47
6	Hanging wall volcanic rocks	37.64	1.96	5.57	0.7	0.69	1.61	0.94	0.15	63.12	3.9	8.34	0.25	23.05	2.87
7	Hanging wall volcanic rocks	37.55	1.97	5.6	0.7	0.7	1.61	0.94	0.15	63.12	3.8	9.34	0.25	23.15	3
8	Hanging wall volcanic rocks	38.64	1.9	5.63	0.6	0.79	1.63	0.9	0.19	60.12	3.9	11.34	0.15	23.15	3
9	Hanging wall volcanic rocks	40.54	1.89	5.64	0.65	0.84	1.64	0.91	0.2	62.12	1.9	8.35	0.15	20.15	2
10	Hanging wall volcanic rocks	38.44	0.79	6.74	0.5	0.99	1.84	0.71	0.19	62.13	2.07	8.3	0.2	22.15	1
11	Ore layers	10.05	0.31	246.8	0.19	0.16	0.36	0.25	0.03	39.52	1.09	39.67	0.47	3.3	0.69
12	Massive ore	18.8	4.9	33	1.6	0.3	1.1	0.4	0.05	1163	1.5	5.2	1.46	1.7	1.8
13	Ore layers	23.9	0.8	192	1.1	0.4	1.3	0.7	0.06	168	2.7	3.5	0.74	65.3	1.8
14	Ore layers	47.25	6.5	14	1.5	0.2	0.65	0.5	0.03	76	0.5	12.9	1.23	20.1	2.1
15	Massive ore	15.9	4.9	128	2.4	0.3	0.9	1.8	0.05	186	10.9	0.72	2.05	0.3	1.3
16	Ore layers	10.8	4.01	134	1.6	0.2	0	0.2	0.01	385	1.3	3.8	0.58	1.6	0.6
17	Ore layers	3.5	2.1	0.98	1.7	0.4	1.8	0.03	0.04	2200	1.2	0.93	0.53	1.9	1.6
18	Massive ore	18.3	3.2	0.25	3.2	0.3	0.3	0.5	0.06	125	1.9	6.3	0.3	1.1	2.9
19	Ore layers	3.8	0.7	0.5	0.4	0.05	7.5	0.09	0.08	1142	0.3	0.9	0.73	2.1	0.8
20	Ore layers	20.3	0.3	32	1.2	0.2	0.9	0.5	0.03	1162	2.6	2.7	1.2	0.2	3

Sample	Rocks	Pb	Ni	Nd	Nb	Mo	Lu	Li	La	In	Ho	Hf	Ge	Gd	Ga
1	Footwall volcanic rocks	4	3	6.5	0.98	0.52	0.39	4.98	3.5	0.07	0.92	1.86	1.23	2.85	15.18
2	Footwall volcanic rocks	1.05	3.66	9.71	1.36	1.8	0.36	6.7	6.58	0.05	0.81	2.08	0.65	3.03	9.85
3	Footwall volcanic rocks	1.99	5.99	10.6	1.41	0.46	0.5	7.05	6.94	0.09	1.06	3.02	1.33	3.7	11.28
4	Footwall volcanic rocks	2.52	5.28	8.24	2.61	0.54	0.18	9.57	10.48	0.03	0.39	1.71	1.38	1.96	14.57
5	Footwall volcanic rocks	1.21	1.68	14.3	4.79	0.59	0.43	9.8	11.95	0.05	1	3.17	0.93	3.97	9.43
6	Hanging wall volcanic rocks	1.37	5.74	13.3	3.1	0.66	0.66	12.96	8.82	0.06	1.48	4.73	1.36	4.68	10.71
7	Hanging wall volcanic rocks	1.38	5.75	13.3	3.1	0.67	0.66	13	8.9	0.07	1.5	4.74	1.4	4.7	10.7
8	Hanging wall volcanic rocks	1.5	5.6	13.4	3	0.76	0.56	13.06	9	0.06	1.58	4.81	1.26	4.78	10.6
9	Hanging wall volcanic rocks	2.4	2.7	16.4	1	0.76	0.56	15.06	11	0.06	0.68	3.71	1.06	4.98	12.6
10	Hanging wall volcanic rocks	1.4	2.08	15.6	2.1	0.66	0.56	14.06	9.99	0.06	0.68	4.01	1.76	4.08	13.5
11	Ore layers	0.76	28.07	3.37	0.32	0.81	0.15	5.36	2.03	0.05	0.37	0.55	0.67	1.32	14.05
12	Massive ore	13.85	39.4	7.9	1.1	77.9	0.3	8.5	9.5	0.02	0.6	1.14	0.39	2.6	10.49
13	Ore layers	11.23	52.21	7.8	0.16	34.8	0.3	6.3	1.8	0.04	0.7	0.07	0.32	4.03	7.68
14	Ore layers	32.36	40.5	52.3	0.96	6.5	0.2	5.3	9.1	0.05	0.5	1.32	0.56	3.5	14.52
15	Massive ore	5.09	21.08	5.9	0.64	1.39	0.4	8.5	7.9	0.09	1.6	0.3	0.14	2	11.2
16	Ore layers	4.67	24.2	2.6	0.22	47.0	0.6	8.6	57.8	0.06	0.4	1.15	0.37	2.3	14.2
17	Ore layers	2.75	99.9	1.2	0.76	7.52	0.2	13.9	3.5	0.03	0.03	1.01	0.62	4.7	8.7
18	Massive ore	5.17	42	8.6	1.34	39.0	0.4	5.3	11.8	0.11	0.7	0.07	0.93	3	10.52
19	Ore layers	2.4	33.06	1.5	0.18	0.04	0.03	7.9	2.8	0.03	0.05	0.03	0.19	0.3	7.64
20	Ore layers	17.2	42.3	13.1	1.53	0.18	0.2	6.2	16.5	0.08	0.6	0.42	0.43	2.9	3.12

Sample	Rocks	Eu	Er	Dy	Cu	Cs	Cr	Co	Ce	Cd	Be	Ba	As
1	Footwall volcanic rocks	0.78	2.57	4.27	53.96	0.01	4.61	17.7	9.04	0.08	0.34	11.95	13.04
2	Footwall volcanic rocks	0.85	2.32	4.02	368.1	0.05	4.88	16.2	16.46	0.05	0.41	30.9	12.9
3	Footwall volcanic rocks	0.77	3.18	5.02	176.1	0.02	8.78	6.39	17.43	0	0.42	18.59	13.63
4	Footwall volcanic rocks	0.62	1.1	1.83	36.15	0.69	14.11	14.4	21.64	0.05	0.74	286.3	13.21
5	Footwall volcanic rocks	1.09	2.77	4.83	84.13	0.34	13.16	2.73	28.03	0.04	0.9	425.5	12.57
6	Hanging wall volcanic rocks	0.83	4.36	7.08	10.7	0.05	20.31	1.1	21.57	0.08	0.77	175.8	12.08
7	Hanging wall volcanic rocks	0.8	4.3	7.08	11.01	0.05	20.07	1.1	21.6	0.08	0.77	176	11.98
8	Hanging wall volcanic rocks	0.94	4.2	7.24	12.7	0.05	18.3	3.1	19.57	0.07	0.79	170.8	17.08

(*continued on next page*)

Table 1 (*continued*)

Sample	Rocks	Eu	Er	Dy	Cu	Cs	Cr	Co	Ce	Cd	Be	Ba	As
9	Hanging wall volcanic rocks	0.94	2.2	7.12	12.8	0.05	18.31	3	19.67	0.06	0.5	172.0	17
10	Hanging wall volcanic rocks	0.7	2	3	12.02	0.05	19	5	16	0.07	0.49	165.0	24
11	Ore layers	0.51	1.09	1.85	1989	0.03	65.35	42.3	5.14	0	0.22	49.7	0
12	Massive ore	0.1	2	2.8	41.1	0.06	40	43.5	9.63	0	0.32	9213	0
13	Ore layers	0.32	2.2	3.2	175.7	0.07	62	20.8	11.01	0	0.73	1250	0
14	Ore layers	0.06	1.6	6.9	509.9	0.03	36	35.3	12.34	0	0.92	149	0
15	Massive ore	0.03	4.02	1.5	129.0	0.05	73	38.0	9.65	0	0.09	5338	0
16	Ore layers	2.7	1.5	1.6	804.3	0.02	28	13.8	7.1	0	0.59	9901	0
17	Ore layers	0.06	1.2	0.4	23.7	4.8	95	2.9	7.35	0	0.03	444	0
18	Massive ore	0.09	2.1	3.1	97.31	0.09	24	36.9	1.82	0	0.67	412	0
19	Ore layers	0.02	0.2	0.3	62.86	0.02	86	2.8	1.5	0	0.52	382	0
20	Ore layers	0.6	1.9	2.8	75.73	1.4	15	5.4	12.32	0	0.31	148	0

Sample	11	12	13	14	15	16	17	18	19	20
Si	26.61	20.53	26.02	27.28	18.6	25.29	29.0	22.56	28.94	31.80
Al	0.77	0.42	0.62	0.29	1.24	1.59	1.53	1.41	0.92	0.57
Fe	2.27	1.53	0.64	1.39	2.1	1.95	1.33	2.1	1.76	1.32
Mn	16.03	33.14	15.71	18.9	30.9	15.17	13.9	22.69	15.24	12.41
Mn/Fe	7.06	21.66	24.54	13.59	14.7	7.77	10.4	10.8	8.65	9.4
Co/Ni	1.5	1.1	0.39	0.87	1.8	0.57	0.02	0.87	0.08	0.12
Co/Zn	0.51	0.92	0.44	1.48	2.86	0.27	0.06	0.33	0.07	0.09

such as selective enrichment of bioessential elements have been widely used to assess the origin of manganese deposits (Shah and Khan, 1999; Nakagawa et al., 2009, 2011; Polgári et al., 2012; Şaşmaz et al., 2014). Among the major oxides, Mn, Fe, Si, Ti and Al contents are very useful to discriminate the origin of manganese ores (Karakus et al., 2010; Sasmaz et al., 2014). Analytical results of the major and trace elements of the Cheshmeh-Frezi Mn deposit is given in Table 1. Based on the analysis of randomly collected 10 ore samples from the deposit, the Mn ores are relatively homogeneous with most samples showing a Mn:Fe ratio largely higher than 1. Manganese ranges from 12.41 to 33.14 wt.% (average = 19.41), and Fe ranges from 0.64 to 2.27 wt.% (average = 1.63) (Table 1). In sedimentary exhalative manganese deposits, iron and manganese are characteristically fractionated, producing high or low Mn/Fe ratios. In general, the range 0.1 < Mn/Fe < 10 holds; whereas in hydrogenous deposits this ratio is closer to unity (Nicholson et al., 1997). The Mn/Fe ratio in the Cheshmeh-Frezi deposit is comparable with those characteristic of sedimentary exhalative deposits, as defined by Nicholson et al. (1997). In the Si versus Al plot used for discriminating hydrothermal and sedimentary types of Mn ores (Toth, 1980; Nicholson, 1992; Mücke et al., 1999; Karakus et al., 2010; Öksüz, 2011; Sasmaz et al., 2014; Wu et al., 2016), our data plot distinctively in the hydrothermal field (Fig. 10A). This is due to the high SiO_2

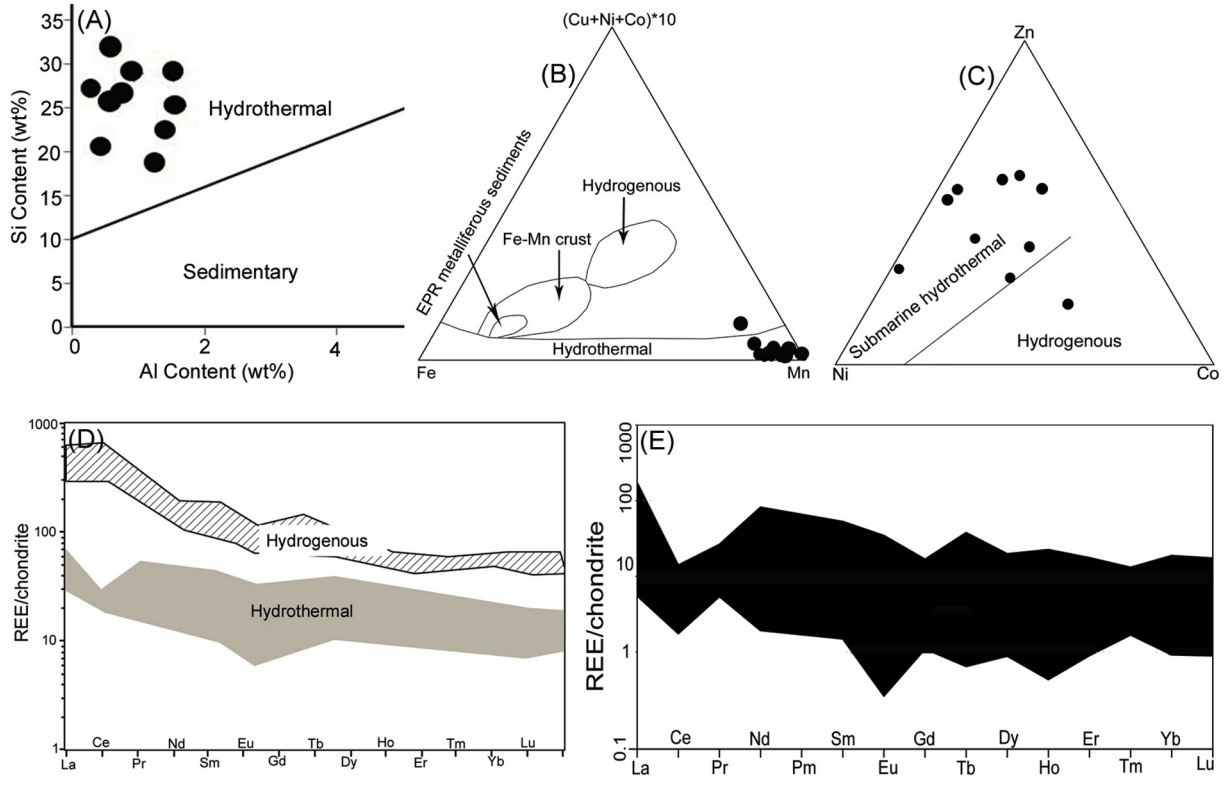

Fig. 10. A: Si-Al discrimination for the Cheshmeh-Frezi samples. The middle line separates hydrothermal and hydrogenous deposits (Toth, 1980). B: Mn–Fe–(Ni + Co + Cu)*10 discrimination diagram (Bonatti et al., 1972; Crerar et al., 1982), B: Zn–Ni–Co discrimination diagram (Choi and Hariya, 1992). D: REE diagram showing hydrogenous and hydrothermal fields (Stackelberg, 1997). E: Chondrite normalized REE (Nakamura, 1974) diagram for ore samples of manganese in the Cheshmeh-Frezi deposit.

content of hydrothermal fluid, with respect to the content of sedimentary formations (Karakus et al., 2010).). However, other parameters such as the presence of biogenic silica, diagenetic components and clastic materials can also explain high Si values, without introducing a hydrothermal component (Toth, 1980; Polgári et al., 2012; Zarasvandi et al., 2013).

The hydrogenous and hydrothermal deposits can be distinguished by using Co/Ni and Co/Zn ratios (Toth, 1980; Sasmaz et al., 2014). A Co/Ni ration lower (or higher) than 1 indicates a sedimentary origin (or a deep marine environment) (Delian, 1994; Fernandez and Moro, 1998; Öksüz, 2011). In the Cheshmeh-Frezi deposit, the Co/Ni ratios range from 0.02 to 1.8 (average = 0.73, n = 10), with three samples showing ratios exceeding 1 (Table 1). Co/Zn ratios of 0.15 indicate hydrothermal-type deposits, while Co/Zn ratios of >2.5 are typical of hydrogenous-type deposits (Toth, 1980). In the Cheshmeh-Frezi Mn deposit, the Co/Zn ratios range from 0.06 to 2.86 (average = 0.70), with one sample giving a value higher than 2.5 (see Table 1). Although Co/Zn ratios point to a hydrothermal source for Mn mineralization, the Co/Ni ratios of ore samples indicate that sedimentary environments also played an important role during the formation of the Cheshmeh-Frezi Mn deposit. The Mn–Fe–(Co + Ni + Cu) (Bonatti et al., 1972; Crerar et al., 1982) and Zn–Ni–Co ternary plots (Choi and Hariya, 1992) are useful to discriminate between hydrothermal and hydrogenous origin of a Mn deposit. All the studied manganese ore samples plot within the hydrothermal field (Fig. 10B and C).

A trace element (As, Ba, Cu, Li, Mo, Pb, Sb, Sr, V, Zn) enrichment is generally observed in oxide ores deposited from hydrothermal fluids (Nicholson, 1992b). In the studied ores, we may observe an enrichment trend of Ba, Cu, Pb, Sr, V, and Zn (see Table 1). However, these values are lower than those reported in hydrogenous deposits but are slightly higher compare to the values of hydrothermal deposits (Adachi et al., 1986; Bonatti et al., 1972; Choi and Hariya, 1992; Crerar et al., 1982; Nicholson, 1992a; Peters, 1988; Shah and Moon, 2007; Toth, 1980; Sasmaz et al., 2014; Brusnitsyn and Zhukov, 2012). In the case of Cheshmeh-Ferzi deposits, the footwall andesitic rock is hosting a Cu-(Zn) sulfide mineralization, probably at the origin of the base metal enrichment of Mn ores. Zn concentrations in the ores range between 13.3 and 111 ppm (average = 51.16); Copper and Lead concentrations in the ores range from 23.7 to 1989.28 ppm (average = 390.89) and 0.76 to 32.36 ppm (average = 9.54), respectively. According to Hein et al. (2008), high Cu, Zn, and Pb concentrations typically reflect the influence of sulfides. Sulfides might precipitate at depth or in the footwall layers and experienced further leaching and fractionation by the fluids at the origin of Mn oxides. For Mo, the high concentrations may reflect leaching only at high temperatures (i.e., >310 °C) in the hydrothermal fluids as well as leaching of acidic to mafic igneous rocks (Hein et al., 2008; Sasmaz et al., 2014). Molybdenum concentrations in the ores range from 0.04 to 77.97 ppm (average = 21.53). Such a low Mo content in the Mn ores may reflect low temperature conditions of hydrothermal fluids. Hydrothermal oxides generally display lower Co content while hydrogenous deposits present higher amounts, which are also indicative of marine environments (Del Rio Salas et al., 2008). Cobalt concentrations of Mn deposit in the Cheshmeh-Frzi range from 2.8 to 43.5 ppm (average = 24.18). These low values suggest a very limited contribution of hydrogenous processes during mineralization. Barium concentrations in the Cheshmeh-Frezi manganese deposit range from 49.7 to 9901 ppm (average = 2728.67) in agreement with the values found in hydrothermal deposits. The Ba content in hydrothermal solutions is usually higher than that of seawater because of the influence of volcanic activity and sedimentation (Monnin et al., 2001; Öksüz, 2011; Sasmaz et al., 2014).

Table 2
Comparison of characteristics between Cheshmeh-Frezi manganese deposit and volcanogenic type manganese deposits.

Deposit characteristics	Franciscan type	Cuban type	Olympic Peninsula type	Cyprus type	Cheshmeh-Frezi
Tectonic setting	Mid-oceanic ridge, inner-arc	Back-arc, island-arc	Mid-plate seamount	Mid-oceanic ridge, back-arc	Back-arc
Depositional environment	Submarine	Submarine	Submarine	Submarine	Submarine
Age of mineralization	Paleozoic to Tertiary	Cambrian to Pliocene	Eocene	Paleozoic to Tertiary	Lower late Cretaceous
Host/associated rock types	Chert, shale, argillite	Tuff, volcanic rocks	Limestone, pillow basalt, agglomerate, argillite, graywacke	Pillow-basalt, pelagic limestone	Red tuff, sandy tuff, andesite, trachyandesite
Deposit form	Concordant with bedding	Tabular, conformable to bedding	Tabular lenses	Lenticular	Blanket-like and tabular
Texture	Colloform, botryoidal, massive	Layer, lamina, disseminated, massive, veinlet	Finely crystalline, massive, Banded, colloform, fecal pellets	Massive, banded, disseminated	Layer, laminae, banded, massive, disseminated, veinlet
Ore mineralogy	Psilomelane, pyrolusite, rhodochrosite, hausmannite, braunite	Psilomelane, pyrolusite, braunite, bementite	Bementite. Hausmannite, neotocite	Amorphous hydroxide of manganese, iron oxide	Psilomelane, pyrolusite, braunite
Gangue mineralogy	Quartz, chalcedony, hematite, calcite, siderite, barite	Quartz, chalcedony, jasper, calcite, siderite, chlorite, feldespars	Quartz, hematite, calcite, minor barite	Iron oxide, pyrite, calcite, chlorite, quartz	Quartz, feldspar, chlorite, lithic clasts
Genesis	Volcanogenic-exhalative	Volcanogenic-exhalative	Volcanogenic-exhalative	Volcanogenic-exhalative	Volcanogenic-exhalative
References	Moser and Page, 1988; Cazanas et al., 1998; Sasmaz et al., 2014; Ozturk, 1997				This study

REE contents of 10 samples collected from the Cheshmeh-Frezi manganese mineralization are shown in Table 1. As the REE contents of hydrothermal and hydrogenous deposits considerably differ (Fig. 10D), they can provide information on the genetic processes involved in the formation of submarine Mn and Fe-Mn ores (Fig. 10D) (Toth, 1980; Hein et al., 1997). Hydrogenous Mn deposits are more enriched in REE compare to the hydrothermal type and they show a clear LREE enrichment. Hydrothermal Mn deposits are characterized by a negative Ce anomaly (Sabatino et al., 2011), which is not observed in the hydrogenous type. All samples of the Cheshmeh-Frezi manganese mineralization show a strong negative Ce anomaly similar to that of submarine hydrothermal deposits (Fig. 10D and E). The Ce anomaly depends on the temperature of the fluid, the proximity to the hydrothermal source, and redox conditions (Hein et al., 1997, 1994; Okuz and Okuyucu, 2014).

7.2. Comparison with other classical volcanogenic Mn deposits

The geology, lithostratigraphy, geometry and geochemical composition of the manganese ores from Cheshmeh-Frezi suggest that mineralization mostly formed from volcanogenic hydrothermal

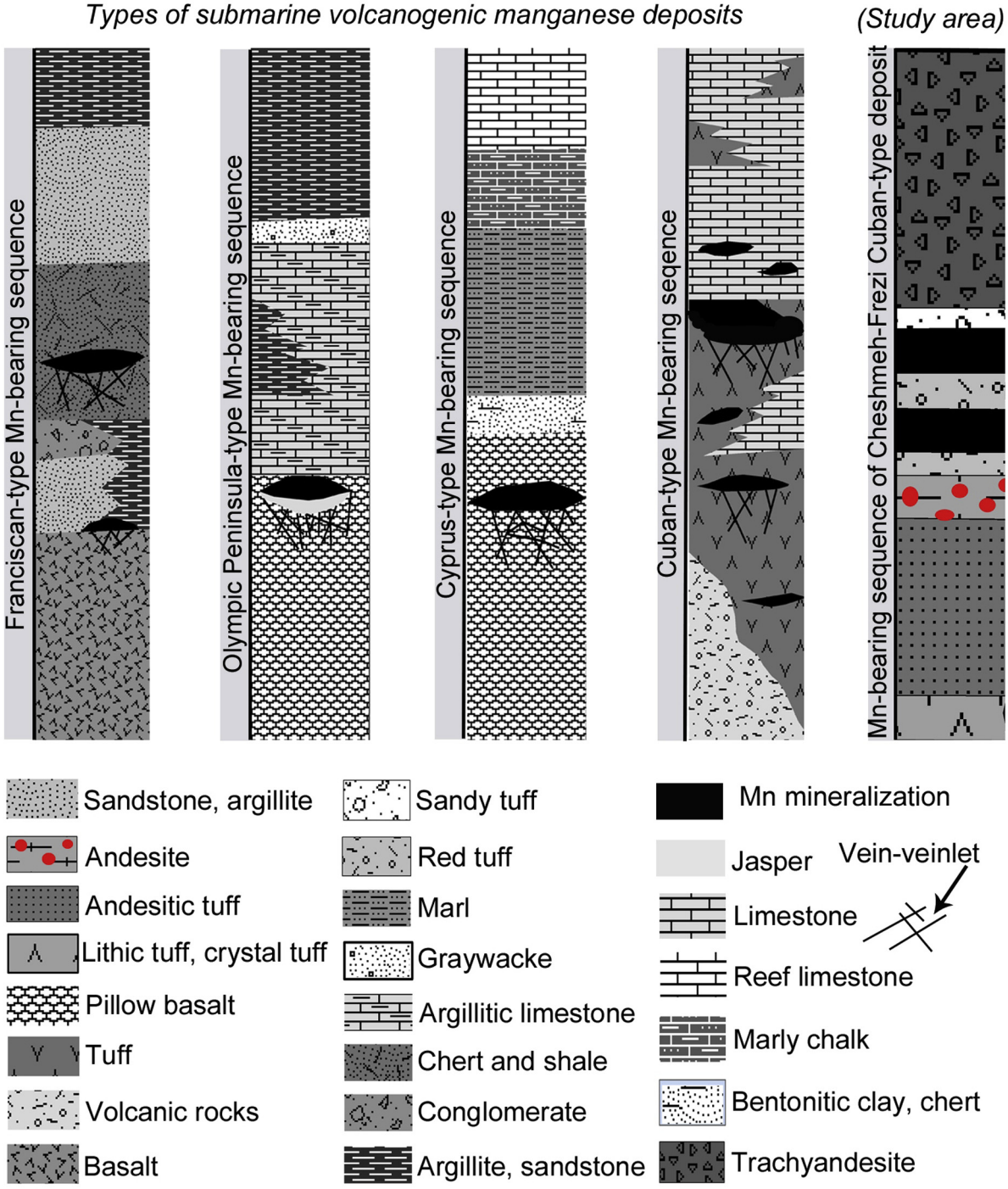

Fig. 11. Lithostratigraphic correlation diagram of the volcanogenic manganese deposits sequence (Moser and Page, 1988) and Mn-bearing sequence in the Cheshmeh-Frezi deposit.

exhalites. Four distinct categories of volcanogenic manganese deposits have been proposed by Moser and Page (1988) based on their tectonic setting, lithostratigraphic sequence and geochemical characteristics: Franciscan type, Cuban type, Olympic Peninsula type and Cyprus type. The characteristics of each of the four types of volcanogenic manganese deposits are discussed below and summarized in Table 2. Generally, these four types occur in different depositional environments and each type shows particular characteristics, whether in volcano-sedimentary sequence, mineralogy, geometry and size.

Generally, ore bodies in the four type deposits are thin, narrow to wide ellipsoids; these shapes suggest a genetic association with linear structural features on the sea floor where the deposits were formed. Lengths and widths among the deposit types differ significantly except for the Cuban and Cyprus type, which are the largest in extent (Moser and Page, 1988). Cyprus type deposits are also significantly thicker than the other deposit types (Moser and Page, 1988; Keith et al., 2016). Length-to-width ratios among the types are similar; for example, Franciscan, Cuban, and Olympic Peninsula deposits are about 3 times as long as they are wide, and Cyprus types about 4 times as long as they are wide. In the Cheshmeh-Frezi deposit, the morphology of the orebodies is stratiform, sheet-like and tabular with length ranging from 800 to 2300 m and thickness between 6 and 20 m (Fig. 5C). This geometry of mineralization was also recognized in the Garab Cuban-type Mn deposit hosted in the Eocene volcano-sedimentary sequence of Alborz zone in Northern Iran (Doulatkhah et al., 2005). The host rocks among the four deposit types are dalso instinct (Table 2). Franciscan type deposits are hosted mostly in white, red, or green massive to thin-bedded chert. Olympic Peninsula deposits are hosted in basalt or in the contact between basalt and limestone. Cyprus-types are hosted in basalt flows and sedimentary rocks, such as caly, marl, chalk, or chert (Jowitt, 2008; Keith et al., 2016). The major host rocks in Cuban-types are pyroclastic rocks, mainly dacitic and andesitic tuff and flows (Figs. 11 and 12B) (Moser and Page, 1988). In Mexico, Cuba and Turkey, tuff is major host rock in at least 80% of deposits (Ozturk, 1997; Del Rio Salas et al., 2008; Sasmaz et al., 2014). Similar to the Cuban-type, the

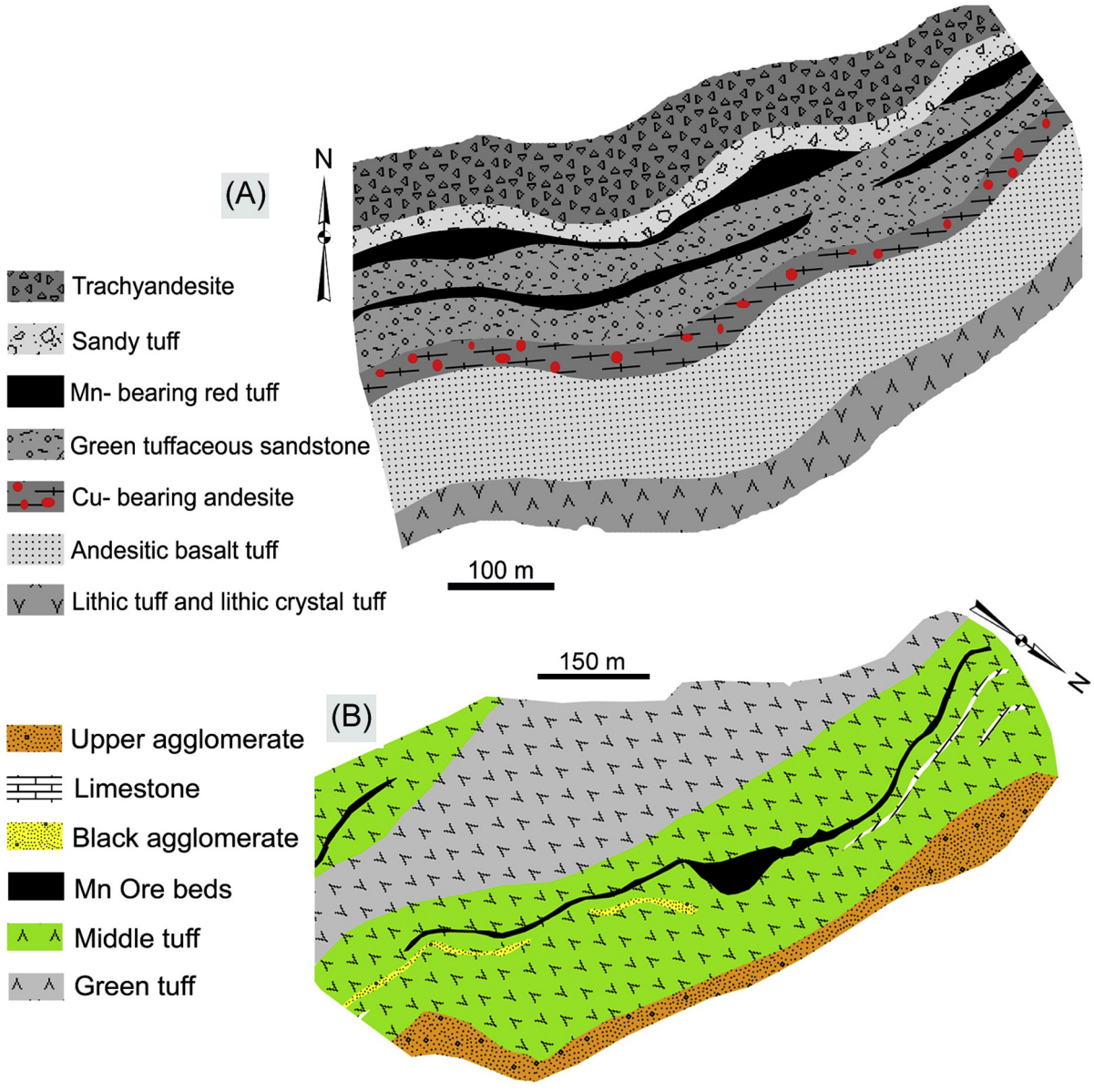

Fig. 12. A: Plan view of the ore-bearing sequence in the Cheshmeh-Frezi deposit. B: Plan view of the ore-bearing sequence in the Cuban-type Mn deposits (modified after Cazanas et al., 1998).

host rocks of mineralization in the Cheshmeh-Frezi deposit are red tuff and associated marine sedimentary rocks including minor sandy tuffs (Figs. 11 and 12A). The association of the Cheshmeh-Frezi mineralization with submarine volcano-sedimentary rocks suggested closer affinities to the Cuban-type deposits.

Another major difference between the different types of Mn, deposits is the absence of a Mn silicate or carbonate mineral in Cyprus deposits; only amorphous manganese hydroxide are reported (Jowitt, 2008). The Cuban-type deposits also differ from both Franciscan and Olympic Peninsula deposits in the paucity or absence of Mn carbonate minerals, such as rhodochrosite or manganocalcite. In the Cuban type deposits, the Mn ore include silicates (braunite, neotocite, and bementite) and oxides (psilomelane, pyrolusite and manganite). In the Cheshmeh-Frezi deposit, ore mineralization comprises psilomelane, pyrolusite and minor braunite.

The Cuban-type deposits in Cuba, Turkey and Iran are limited to certain units. They may be strata-bound, but usually they are con-

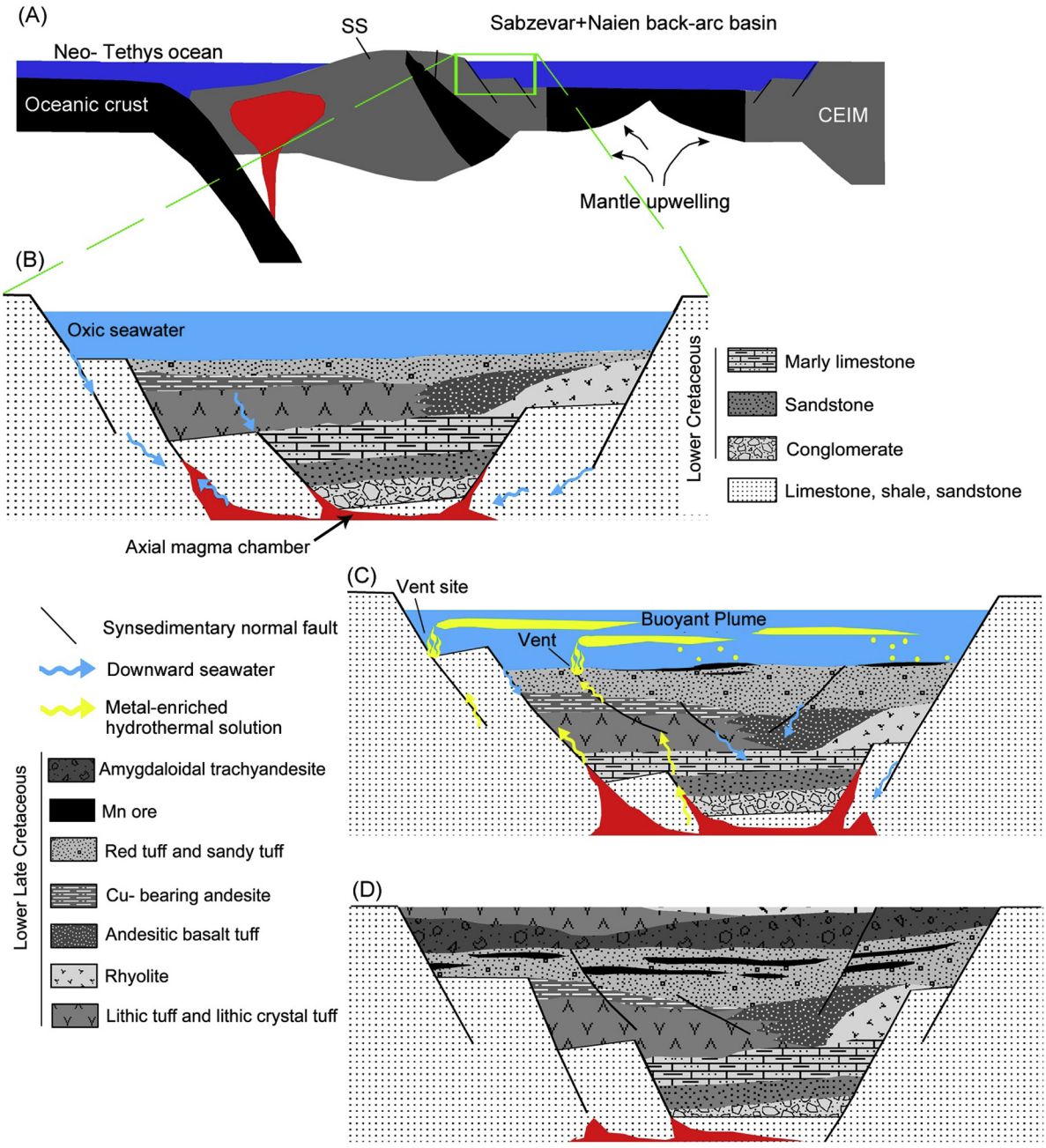

Fig. 13. Relation between manganese mineralization and tectono-magmatic evolution of the area based on geodynamic models proposed by Rossetti et al. (2010), A. During the Late Cretaceous, intraoceanic subduction developed within the Neotethys. Later on, renewed back-arc extension caused formation of the Sabzevar- Naien ocean in the upper-plate of the Neotethyan subduction, concurrently with the main phase of magmatism in the Sanandaj–Sirjan Zone. Southwest Sabzevar bimodal volcanism and formation of the manganese mineralization and Besshi-type VMS deposits within this volcano–sedimentary basin occurred in this time (Maghfouri et al., 2016). B: During this episode, coarse grained detrital sedimentary rocks and intense bimodal volcanism formed linked to submarine volcanism in the initial stage of the back-arc rifting. C: In this stage, seawater penetrates to depth; it reacts with magma producing a hot, strongly reduced and acidic hydrothermal fluid. D: The resultant hydrothermal solutions are transported upwards, commonly along fault structures and eventually disperse in the seawater or precipitate metals (Mn) forming mineral deposit. In this stage of mineralization, Cheshmeh-Frezi manganese deposit formed.

formable to bedding and stratiform (Moser and Page, 1988; Ozturk, 1997; Doulatkhah et al., 2005; Sasmaz et al., 2014). This suggests that mineralization is stratigraphicaly controlled by layers (Fig. 12B) Mineralization in the Cheshmeh-Frezi deposit is also restricted to red tuff and sandy tuff rocks (Figs. 4A, 5A and 12A). The occurrence of the layer-hosted mineralization in the tuff rocks indicates that there is a strong stratigraphic control on the deposition of the mineralization in the Cheshmeh-Frezi deposit (Figs. 4, 5A and 11).

Franciscan and Cyprus type deposits are believed to have formed on the ocean floor at the rock-seawater interface by solutions emanating from fractures at or near a mid-oceanic ridge or in a rifted basin. Olympic Peninsula type deposits formed similarly on or around seamounts in an ocean basin. Cuban type manganese deposits are associated with intermediate to felsic island-arc volcanic rocks and are thought to have formed from sea-floor hot spring in shallow marine back-arc environments (Table 2) (Moser and Page, 1988). Based on the bimodal nature of volcanism, the regional geologic setting (Maghfouri, 2012; Maghfouri et al., 2016) and the petrographic and geochemical features of the foot- and hanging-wall volcanic rocks, we suggest that manganese mineralization in the Cheshmeh-Frezi formed in a back-arc basin (Fig. 13A). Characteristic features of the Cheshmeh-Frezi deposit, including its occurrence within a volcano-sedimentary sequence, strata-bound and strati-form ore bodies hosted by tuff rocks, ore mineralogy composed of psilomelane, pyrolusite and braunite, a back-arc basin for tectonic setting, indicate that the Cheshmeh-Frezi deposit is equivalent to Cuban-type manganese deposits.

7.3. Genetic model and depositional environment of Cheshmeh-Frezi deposit

Geochemical constraints from volcanic rocks and stratigraphic features of the LLCVSS suggest that the most likely tectonic setting for the southwest Sabzevar basin was a continental back-arc basin, that developed northeast of the Sanandaj–Sirjan Zone (Fig. 13A) (Rossetti et al., 2010; Maghfouri et al., 2016).

Continental back-arc settings contain some of the world's most economically important Mn and VMS districts (Franklin et al., 2005; Galley, 2003; Sasmaz et al., 2014; Rajabi et al., 2014; Maghfouri et al., 2016). According to the stratigraphy of the late Cretaceous volcano-sedimentary sequence, the ore deposits of the southwest Sabzevar basin (Mn and Besshi-type VMS) formed during different stages of the basin evolution (Fig. 13) (Maghfouri et al., 2016), which may be described as follows. The subduction of the Neotethys oceanic crust under the Central Iranian microcontinent has been followed by continental margin back arc rifting (Fig. 13A) and by the deposition of a *syn*-rift sequence during the Lower Cretaceous (Fig. 13B). It is indicated by coarse grained detrital sedimentary rocks and intense bimodal volcanism (unit 1). During this episode, stratiform Mn formed linked to submarine volcanism in an initial stage of back-arc rifting (Maghfouri et al., 2016). Cheshmeh-Frezi, Nudeh, Benesbourd and Goft Mn deposits and oxide Cu mineralization (Garab occurrence) formed during this stage (Maghfouri et al., 2016). These stratiform Mn deposits, distributed in LLCVSS are contemporaneous and spatially associated with submarine volcanism in the back-arc basin (Maghfouri et al., 2016). However, the generally low Fe/Mn ratios and the low concentrations of trace elements and REE of Mn oxide from the Cheshmeh-Frezi deposit suggest that this deposit probably formed due to submarine hydrothermal activity.

The downward circulation of seawater through a fractured oceanic crust (Fig. 13C) (or normal *syn*-sedimentary fault) led to progressive warming and reduction (through volcanogenic heat source) and an increase in acidity that convert the seawater to low-intensity (<200 °C) and high-intensity (>200 °C to ca.400 °C) hydrothermal solutions able to leach Mn and different elements from the surrounding volcanic rocks (Roy, 1992). The metal-enriched hydrothermal solution was further convected upward to the sea floor at or near the sub-seafloor (Fig. 13D). Deposition of different metals resulted from decreasing of pressure and temperature and increasing of Eh and/or pH in the solution. Cooling of the hydrothermal solution may occur during conduction process and/or by subsurface mixing with seawater (~2 °C). The process at the origin of the manganese mineralization of the Lower Cretaceous Cheshmeh-Frezi deposit is somehow very similar to what is currently observed in modern hydrothermal systems within the active extensional basin,

The variation in the Mn/Fe ratio in the different manganese deposits can be explained either by the original ratio in the solution or by the relative efficiencies of the competing processes of in situ precipitation and advection of the metals away from the vents (Roy, 1992). The stability limits of Fe-Mn compounds show that Fe minerals generally precipitates as first, close to the source, whereas Mn maintains a longer residence time in the solution (Choi and Hariya, 1992). The fractionation between Mn and Fe suggests a spatial variation of Eh and/or pH pareemter relative to the site of deposition in the study area. The absence of Fe minerals in the Cheshmeh-Frezi deposit, suggest high fractionation between Fe and Mn and may support the hypothesis that this deposit formed at a considerable distance from hydrothermal venting zones.

8. Conclusions

Manganese mineralization in the Cheshmeh-Frezi is hoosted by red tuff of a volcano-sedimentary sequence (LLCVSS), which was formed predominantly by pyroclastic and volcanic rocks. The Cheshmeh-Frezi deposit occurs as lenses and thin layers. Lithological and geochemical characteristics suggest that the rocks forming the LLCVSS were deposited in a back-arc basin environment. The Mn ore mineralogy, together with major, trace, and REE geochemistry support a hydrothermal origin for this deposit. Magmatism during the evolution of the southwest Sabzevar basin could have triggered the convection of geothermal water and promoted leaching of the footwall rocks that further resulted in the formation of Mn mineralization in the Cheshmeh-Frezi deposit. The chemical composition is characteristic of a hydrothermal origin including 1) a strong fractionation between Fe and Mn for the stratiform Mn, 2) low trace metal contents and 3) low rare earth element contents. Because of the nature of the host rocks, the geometry of the mineralized lenses and the lack of alteration in wall rocks, the ore deposition style is sedimentary exhalative, and it very consistent with the Cuban-typ Mn deposits.

Acknowledgements

Tarbiat Modares University of Tehran provided financial support for this research. We sincerely thank two anonymous journal reviewers for carefully reviewing the manuscript and for their constructive comments. The manuscript has benefited from careful editorial handling by Prof. D. Lentz. We also acknowledge Prof. F. Pirajno Editor-in-Chief of Ore Geology Reviews Journal.

References

Adachi, M., Yamamoto, K., Sugisaki, R., 1986. Hydrothermal chert and assoicated siliceous rocks from the northern Pasific: their geological significance as indication of ocean ridge activity. Sediment. Geol. 47, 125–148.

Aghanabati, A., 1998. Major sedimentary and structural units of Iran (map). Geosciences 7, 29–30.

Aghanabati, A., 2004. Geology of Iran: Geological Survey of Iran, 600.

Ahmadi, A.A., 2006. Mineralogy, geochemistry, facies analysis and genesis of the Fe – Mn ore deposits in south east of Torbat Heydarieh [Unpublished M.Sc. thesis]. University of Tarbiat Modares, Iran, p. 187 (in Persian with English abstract).
Alavi, M., 1996. Tectonostratigraphic synthesis and structural style of the Alborz Mountains system in northern Iran. J. Geodyn. 11, 1–33.
Amiri, A., 1995. Geology, mineralogy and controlling factors of formation and concentration of ore matter in Robat Karim manganese deposit, SW Tehran-Iran [Unpublished M.Sc. thesis]. University of Tarbiat Modares, Iran, p. 200 (in Persian with English abstract).
Arvin, M., Robinson, P.T., 1994. The petrogenesis and tectonic setting of lavas from the Baft ophiolitic Melange, southwest of Kerman, Iran. Canadian J. Earth Sci. 31, 824–834.
Asiabanha, A., Bardintzeff, J.M., Kananian, A., Rahimi, G., 2012. Post-Eocene volcanics of the Abazar district, Qazvin, Iran: mineralogical and geochemical evidence for a complex magmatic evolution. J. Asian Earth Sci. 45.
Barrett, T.J., MacLean, W.H., 1999. Volcanic sequences, lithogeochemistry, and hydrothermal alteration in some bimodal volcanic-associated massive sulfide systems. Rev. Econ. Geol. 8, 101–131.
Betts, P.G., Lister, G.S., O'Dea, M.G., 1998. Asymmetric extension of the Middle Proterozoic lithosphere, Mount Isa terrane, Queensland, Australia. Tectonophysics 296, 293–316.
Bonatti, E., Kraemer, T., Rydel, H., 1972. Classification and genesis of submarine iron– manganese deposits. In: Horn, D.R. (Ed.), Ferromanganese Deposits on the Ocean Floor. Natl. Sci. Found., Washington, D. C., pp. 149–166.
Bonyadi, Z., Moore, F., 2005. Geochemistry and genesis of Narigan ferromanganese deposit, Bafgh, Yazd province. J. Earth Sci. Iran 57 (in Persian with English abstract).
Brusnitsyn, A.I., Zhukov, G.I., 2012. The South Faizuly Manganese Deposit in the Southern Urals: Geology, Petrography, and Formation Conditions. Lithol. Min. Resour. 40 (1), 30–47.
Cazanas, X., MelgareJo, J.C., Alfinso, P., Escusa, A., Cuba, S., 1998. A model of volcanogenic manganese deposit from the Paleogene volcanic island arc of Cuba: the case of the Cristo-ponupo-Loschivos region. Act Geologica Hispanica 33 (1–4), 239–276.
Choi, J.H., Hariya, Y., 1992. Geochemistry and depositional environment of Mn oxide deposits in the Tokora Belt, norteastern Hokkaido, Japan. Econ. Geol. 87, 1265–1274.
Crerar, D.A., Namson, J., Chyi, M.S., Williams, L., Feigenson, M.D., 1982. Manganiferous cherts of the Franciscan assemblage: I. General geology, ancient and modern analogues, and implications for the hydrothermal convection at oceanic spreading centers. Econ. Geol. 77, 519–540.
Del Rio Salas, R., Ruiz, J., Ochoa-Landin, L., Noriega, O., Bara, F., Meza-Figueroa, D., Paz- Moreno, F., 2008. Geology, geochemistry and Re–Os systematics of manganese deposits from the Santa Rosalia Basin and adjacent areas in Baja California Sur, Mexico. Miner. Deposita 43, 467–482.
Delian, F., 1994. Geological and Geochemical Research of the Manganese Ore Bed (in Chinese), M1. Weather Publishing Press, Beijing.
Doulatkhah, R., Rastad, E., Emami, M.H., 2005. Garab stratiform manganese deposit in the Oligo miocene volcano-sedimentary sequence, northeast of Taleghan (central Alborz). J. Earth Sci. 56 (in Persian with English abstract).
Emamalipour, A., 2010. Mineralogy and genesis of Mn-Fe mineralization in the ophiolite, Chaldoran, NW Iran. J. Crystal. Mineral., Iran 1 (in Persian with English abstract).
Emami, M.H., Sadeghi, M.M., Omrani, S.J., 1993. Magmatic Map of Iran. Geological Survey of Iran.
Fernandez, A., Moro, M.C., 1998. Origin and depositional environment of Ordovician stratiform iron mineralization from Zamora (NW Iberian Peninsula). Miner. Deposita 33, 606–619.
Frakes, L., Bolton, B., 1992. Effects of ocean chemistry, sea level, and climate on the formation of primary sedimentary manganese ore deposits. Econ. Geol. 87 (5).
Franklin, J.M., Gibson, H.L., Jonasson, I.R., Galley, A.G., 2005. Volcanogenic massive sulphide deposits, The Economic Geology Publishing Company, 100th Anniversary Volume, pp. 523–560.
Galley, A.G., 2003. Composite synvolcanic intrusions associated with Precambrian VMS-related hydrothermal systems. Miner. Deposita 38, 443–473.
Hein, J.R., Yeh, H.W., Gunn, S.H., Gibbs, A.E., Wang, C.H., 1994. Composition and origin of hydrothermal ironstones from central Pacific seamounts. Geochim. Cosmochim. Acta 58, 179–189.
Hein, J.R., Koschinsky, A., Halbach, P., Manheim, F.T., Bau, M., Kang, J.-K., Lubick, N., 1997. Iron and manganese oxide mineralization in the Pacific. In: Nicholson, K., Hein, J.R., Buhn, B., Desgupta, S. (Eds.), Manganese Mineralization: Geochemistry and Mineralogy of Terrestrial and Marine Deposits, vol. 119. Geological Society Special Publication, pp. 123–138.
Hein, J.R., Schulz, M.S., Dunham, R.E., Stern, R.J., Bloomer, S.H., 2008. Diffuse flow hydrothermal manganese mineralization along the active Mariana and southern Izu-Bonin arc system, western Pacific. J. Geophys. Res. 113.
Heshmatbehzadi, K., Shahabpour, J., 2010. Metallogeny of manganese and ferromanganese ores in Baft ophiolitic Mélange, Kerman, Iran. Aust. J. Basic Appl. Sci. 4, 302–313.
Hosseini, S.R., Mousivand, F., 2016. Major, trace and rare earth elements (REE) geochemical studies and origin of Sardar manganese deposit in the Foroumad area, East of Shahrood. In: 34th Symposium on Iranian Geosciences. Tehran, Iran (in Persian with English abstract).
Irvine, T.N., Baragar, W.R.A., 1971. A guide to the chemical classification of the common volcanic rocks. Canadian J. Earth Sci. 8, 523–548.
Jowitt, M.S., 2008. Field, petrological and geochemical constraints on the release of base metals into hydrothermal fluids in Cyprus-type Volcanogenic Massive Sulphide (VMS) systems: an investigation of the Spilia- Kannavia epidosite zone, Troodos ophiolite, Cyprus. PhD thesis, University of Leicester.
Karakus, A., Yavuz, B., Koc, S., 2010. Mineralogy and major trace element geochemistry of the haymana manganese mineralizations, Ankara, Turkey. Geochem. Int. 48, 1014–1027.
Keith, M., Haase, M.K., Klemd, R., Krumm, S., Strauss, H., 2016. Systematic variations of trace element and sulfur isotope compositions in pyrite with stratigraphic depth in the Skouriotissa volcanic-hosted massive sulfide deposit, Troodos ophiolite, Cyprus. Chem. Geol. 423, 7–18.
Kuleshov, V.N., 2011. Manganese deposits: communication 2. Major epochs and phases of manganese accumulation in the earth's history. Lithol. Min. Resour. 46 (6), 546–565.
Large, R.R., Bull, S.W., Selley, D., Yang, J., Cooke, D.R., Garven, G., McGoldrick, P.J., 2002. Controls on the Formation of Giant Stratiform Sediment-hosted Zn–Pb–Ag Deposits: With Particular Reference to the North Australian Proterozoic. 4. CODES Special Publication, Hobart, Australia, pp. 107–149.
Maghfouri, S., 2012. Geology, Mineralogy, Geochemistry and Genesis of Cu Mineralization within Late Cretaceous Volcano-Sedimentary Sequence in Southwest of Sabzevar, with emphasis on the Nodeh Deposit, [Unpublished M.Sc. thesis]: University of Tarbiat Modares, Iran, pp. 312 (in Persian with English abstract).
Maghfouri, S., Rastad, A., Mousivand, F., 2015. Stratigraphic position, origin and characteristics of manganese mineralization horizons in the Late Cretaceous volcano-sedimentary sequence, south-southwest of Sabzevar. Journal of Economic Geology, Iran, 6(2) (in Persian with English abstract).
Maghfouri, S., Rastad, A., Mousivand, F., Lin, Y., Zaw, Kh., 2016. Geology, ore facies and sulfur isotopes geochemistry of the Nudeh Besshi-type volcanogenic massive sulfide deposit, southwest Sabzevar basin, Iran. J. Asian Earth Sci. 125, 1–21.
Mahdavi, M., Dabiri, R., Shah Hosseini, E., 2015. Magmatic evolution and compositional characteristics of tertiary volcanic rocks associated with the Venarch manganese mineralization, SW Qom, central Iran. Earth Sci. Res. J. 19 (2).
Malekghasem, F., and Simmonds, V., 2006. Investigation of manganese mineralization in Jokandy, southwest of Hashtrood. J. Earth Sci., Iran; No 63 (in Persian with English abstract).
Masoudi, M., 2008. Geology, mineralogy, geochemistry and genesis of Benesbourd Mn deposit in the southwest Sabzevar. M.Sc. Thesis, Tehran Islamic Azad University, Iran, 100 pp. (in Persian with English abstract).
Meschede, M., 1986. A method of discriminating between different types of mid-ocean ridge basalts and continental tholeiites with the Nb-Zr-Y diagram. Chem. Geol. 56, 207–218.
Monnin, C., Wheat, C.G., Dupre, B., Elderfield, H., Mottl, M.J., 2001. Barium geochemistry in sediment pore waters and formation waters of the oceanic crust on the eastern flank of the Juan de Fuca Ridge (ODP Leg 168). Geochem. Geophys. Geosyst. 2 (1), 1008 (15 pp).
Moser, L.D., and Page, N.J., 1988. Descriptive and grade- tonnage models of volcanogenic manganese deposits in oceanic environments- a modification, U.S Geological Survey.
Mücke, A., Adjimah, K., Annor, A., 1999. Mineralogy, petrography, geochemistry and genesis of the Paleoproterozoic Birimian manganese-formation of Nsuta/Ghana. Miner. Deposita 34, 297–311.
Nabatian, Gh., Rastad, E., Neubauer, F., Honarmand, M., Ghaderi, M., 2015. Iron and Fe-Mn mineralisation in Iran: implications for Tethyan metallogeny. Aust. J. Earth Sci. 62, 211–241.
Nakagawa, M., Santosh, M., Maruyama, S., 2009. Distribution and mineral assemblages of bedded manganese deposits in Shikoku, Southwest Japan: implications for accretion tectonics. Gondwana Res. 16, 609–621.
Nakagawa, N., Santosh, M., Maruyama, S., 2011. Manganese formations in the accretionary belts of Japan: Implications for subduction–accretion process in an active convergent margin. J. Asian Earth Sci. 42, 208–222.
Nakamura, N., 1974. Determination of REE, Ba, Fe, Mg, Na, and K in carbonaceous and ordinary chondrites. Geochim. Cosmochim. Acta 38, 757–775.
Nasrollahi, S., Mousivand, F., Ghasemi, H., 2012. Nudeh Mn deposit in the upper Cretaceous volcano- sedimentary sequence, Sabzevar sub-zone. 31 Th Symposiums on Geosciences, Geological Survey of Iran, Tehran, Iran. (in Persian).
Nicholson, K., 1992a. Contrasting mineralogical–geochemical signatures of manganese oxides' guides to metallogenesis. Econ. Geol. 87, 1253–1264.
Nicholson, K., 1992b. Genetic types of manganese oxide deposits in scotland: Indicators of paleoocean-spreading rate and a Devonian geochemical mobility boundary. Econ. Geol. 87, 1301–1309.
Nicholson, K., Nayak, V.K., Nanda, J.K., 1997. Manganese ores of the Ghoriajhor-Monmunda area, Sundergarh District, Orissa, India: geochemical evidence for a mixed Mn source. Geol. Soc. Lond. Spec. Pub. 119, 117–121.
Öksüz, N., 2011. Geochemical characteristics of the Eymir (Sorgun-Yozgat) manganese deposits, Turkey. J. Rare Earths 29 (3), 287–296.
Okuz, N., Okuyucu, N., 2014. Mineralogy, geochemistry, and origin of Buyukmahal manganese mineralization in the Artova ophiolitic complex, Yozgat, Turkey. J. Chem. 2014.
Ozturk, H., 1997. Manganese deposits in Turkey: distribution, types and tectonic setting. Ore Geol. Rev. 12, 187–203.

Pearce, J.A., 1983. Role of sub-continental lithosphere in magma genesis at destructive plate margins. In: Hawkesworth, C.J., Norry, M.J. (Eds.), Continental Basalts And Mantle Xenoliths, Nantwich, Shiva, pp. 230–249.
Pearce, J.A., 2010. An overview of petrochemistry in the regional exploration for volcanogenic massive sulphide (VMS) deposits. Geochem. Explor. Environ. Anal. 10, 1–18.
Pearce, J.A., 2011. The setting, style, and role of magmatism in the formation of volcanogenic massive sulfide deposits. Miner Deposita 46, 449–471.
Peter, J.M., Scott, S.D., 1999. Windy Craggy, northwestern British Columbia: the world's largest Besshi deposit. Rev. Economic Geol. 8, 261–295.
Peter, M., Leyboune, M., Scott, D., Gorton, M., 2014. Geochemical constraints on the tectonic setting of basaltic host rocks to the Windy Craggy Cu-Co-Au massive sulphide deposit, northwestern British Columbia. Int. Geol. Rev. 56 (12), 1484–1503.
Peters, T., 1988. Geochemistry of manganese-bearing cherts assoicated with Alpine ophiolites and the Hawasina formations in Oman. Mar. Geol. 84 (3–4), 229–238.
Polgári, M., Hein, J.R., Vigh, T., Szabó-Drubina, M., Fórizs, I., Bíró, L., Müller, A., Tóth, A.L., 2012. Microbial processes and the origin of the Úrkút manganese deposit, Hungary. Ore Geol. Rev. 47, 87–109.
Rajabi, A., Canet, C., Rastad, E., Alfonsa, P., 2014. Basin evolution and stratigraphic correlation of sedimentary-exhalative Zn–Pb deposits of the Early Cambrian Zarigan-Chahmir Basin, Central Iran. Ore Geol. Rev. 64, 328–353.
Rajabzadeh, M.A., Haddad, F., Polgari, M., Fintor, K., Walter, H., Molnar, Z., Gyollai, I., 2017. Investigation on the role of microorganisms in manganese mineralization from Abadeh-Tashk area, Fars Province, southwestern Iran by using petrographic and geochemical data. Ore Geol. Rev. 80, 229–249.
Rossetti, F., Nasrabady, M., Vignaroli, G., Theye, T., Gerdes, A., Razavi, m., Moin Vaziri, H., 2010. Early Cretaceous migmatitic mafic granulites from the Sabzevar range (NE Iran): implications for the closure of the Mesozoic peri-Tethyan oceans in central Iran. Terra Nova 22, 26–34.
Roy, S., 1992. Environment and processes of manganese deposition. Econ. Geol. 87, 1218–1236.
Roy, S., 1997. Genetic diversity of manganese deposition in the terrestrial geological record. In: Nicholson, K., Hein, J.R., Buhn, B., Dasgupta, S. (Eds.), Manganese Mineralization: Geochemistry and Mineralogy of Terrestrial and Marine Deposits. Geological Society, London, pp. 5–27 (Special Publication 119).
Roy, S., 2006. Sedimentary manganese metallogenesis in response to the evolution of the Earth system. Earth Sci. Rev. 77, 273–305.
Sabatino, N., Neri, R., Bellanca, A., Jenkyns, H.C., Masetti, D., Scopelliti, G., 2011. Petrography and high-resolution geochemical records of Lower Jurassic manganese-rich deposits from Monte Mangart, Julian Alps. Palaeogeogr. Palaeoclimatol. Palaeoecol. 299, 97–109.
Sasmaz, A., Turkyilmaz, B., Ozturk, N., Yavuz, F., Kumral, M., 2014. Geology and geochemistry of Middle Eocene Maden complex ferromanganese deposits from the Elazığ-Malatya region, eastern Turkey. Ore Geol. Rev. 56, 352–372.
Shah, M.T., Khan, A., 1999. Geochemistry and origin of Mn-deposits in the Waziristan ophiolite complex, north Waziristan, Pakistan. Miner. Deposita 34, 697–704.
Shah, M.T., Moon, C.J., 2007. Manganese and ferromanganese ores from different tectonic settings in the NW Himalayas, Pakistan. J. Asian Earth Sci. 29, 455–465.
Stackelberg, U.V., 1997. Growth history ofmanganese nodules and crusts of the Peru Basin". Geol. Soc. 119, 153–176.
Taghizadeh, S., Mousivand, F., Ghasemi, H., 2012. Zakeri Mn deposit, example of exhalative mineralization in the southwest Sabzevar. 31th Symposium on Geosciences, Geological Survey of Iran, Tehran, Iran. (in Persian).
Tarney, J., Wood, D.A., Saunders, A.D., Cann, J.R., Varet, J., 1980. Nature of mantle heter.
Toth, J.R., 1980. Deposition of submarine crusts rich in manganese and iron. Geol. Soc. Am. Bull. 91, 44–54.
Winchester, J.A., Floyd, P.A., 1977. Geochemical discrimination of different magma series and their differentiation products using immobile elements. Chem. Geol. 20, 325–343.
Wood, D.A., 1980. The application of a Th–Hf–Ta diagram to problems of tectonomagmatic classification and to establishing the nature of crustal contamination of basaltic lavas of the British Tertiary volcanic province. Earth Planet. Sci. Lett. 50, 11–30.
Wu, C., Zhang, Z., Xiao, J., Fu, Y., Shao, S., Zheng, C., Yao, J., Xiao, Ch., 2016. Nanhuan manganese deposits within restricted basins of the southeastern Yangtze Platform, China: Constraints from geological and geochemical evidence. Ore Geol. Rev. 75, 76–99.
Zarasvandi, A., Lentz, D., Rezaei, M., Pourkaseb, H., 2013. Genesis of the Nasirabad manganese occurrence, Fars province, Iran: Geochemical evidences. Chemie der Erde – Geochem. 73 (4), 495–508.
Zarasvandi, A., Rezaei, M., Sadeghi, M., Pourkaseb, H., Sepahvand, M., 2016. Rare-earth element distribution and genesis of manganese ores associated with Tethyan ophiolites, Iran: a review. Mineral. Mag. 80 (1), 127–142.
Zarasvandi, A., Pourkaseb, H., Sepahvand, M., Raith, J., Rezari, M., 2016. Tracing of hydrothermal ore forming process in the Sorkhvand manganese deposit, Kermanshah Province, Iran. Arab J. Geosci. 9, 109.